DOUBLE-DIFFERENCE RELOCATION OF EARTHQUAKES AT UTURUNCU VOLCANO, BOLIVIA, AND INTERIOR ALASKA

By

Laura Hutchinson

RECOMMENDED:

Dr. Jeffrey Freymueller

Dr. Douglas Christensen

Dr. Michael West
Advisory Committee Chair

Dr. Sarah Fowell
Chair, Department of Geosciences

APPROVED:

Dr. Paul Layer
Dean, College of Natural Science and Mathematics

Dr. John Eichelberger
Dean of the Graduate School

11 August 2015
Date

DOUBLE-DIFFERENCE RELOCATION OF EARTHQUAKES AT UTURUNCU VOLCANO, BOLIVIA, AND INTERIOR ALASKA

A

THESIS

Presented to the faculty

of the University of Alaska Fairbanks

in Partial Fulfillment of the Requirements

for the degree of

MASTER OF SCIENCE

By

Laura Hutchinson, B.S.

Fairbanks, Alaska

August 2015

Abstract

In order to reliably interpret seismic patterns, we must have reliable earthquake locations. To improve our catalog locations, I incorporate cross-correlations into double-difference earthquake relocations to generate high precision relative locations. I perform relocations for two regions, one volcanic and one tectonic.

At Uturuncu volcano, I incorporate a wealth of previous studies to present a picture of the processes at play. Seismic, gravity, InSAR, and electromagnetic studies all show that there is a magma body underlying the entire region, and chemical studies suggest that this magma body (the Altiplano-Puna Magma Body, or APMB) is the source of the large ignimbrite eruptions that have occurred in the past. The recent uplift has been modeled as a new batch of magma rising off the APMB, beginning the ascent as a diapir. My relocation results indicate that the seismicity aligns with the top of one of the imaged low velocities zones, which I interpret as a diapir beneath Uturuncu. The earthquakes mark the depth at which the crust is cool enough for brittle deformation. I also perform cross-correlations to determine families of similar events. These families are located around the summit of Uturuncu and display a radial pattern. This suggests that they are due to local volcanic stresses, such as inflation of the volcano, rather than regional stresses.

In Interior Alaska, I study a region that is very seismically active, yet has no mapped Holocene faults. There are a series of seismic zones in the area, each comprised of NNE-striking seismic lineations. I perform earthquake relocations on 40 years worth of seismicity in order to refine and interpret fault planes. I additionally examine three earthquake sequences in the Minto Flats Seismic Zone (MFSZ). These earthquakes are large enough ($\geq$M5) to produce an aftershock sequence to map out the rupture plane. I find that two of the three earthquakes occurred on WNW-striking planes, roughly perpendicular to the dominant direction of the seismic zone. The third earthquake ruptured along a NNE-striking plane but generated a WNW-ESE halo of aftershocks, suggesting that the basement is highly fractured in the region. The NW pattern that I find for the three sequences falls in line with my findings for the rest of the Interior: there are a series of NE-striking faults that are cut by NW-striking faults. Throughout the Interior, these faults cross at approximately 60°, suggesting that they are conjugate faults. I

believe that the three earthquake sequences in the MFSZ are also conjugate faults and are a part of the broader conjugate system throughout the Interior.

Table of Contents

List of Figures

Page

List of Tables

Page

Acknowledgements

I would like to thank Michael West, my advisor, for providing me the opportunity to move to Alaska to study earthquakes. Thanks for sending me to Bolivia and Chile as a part of the PLUTONS project, and for giving me the chance to do field work with the Alaska Earthquake Center. Your encouragement and support, as well as your willingness to let me get distracted by a new earthquake, are very appreciated.

I would also like to thank my other committee members, Jeff Freymueller and Doug Christensen, for their input into the projects. Jeff, thanks for teaching me how to code and providing insights into how an organization like AVO is run. Being a part of AVO gave me the opportunity to see firsthand how important it is to use different types of data and observations in tandem. Doug, thanks for the great company. You helped generate a welcome and friendly atmosphere, one that I am sure to miss.

And, while Carl Tape was not on my committee, he provided a huge amount of support for my thesis. So thank you, Carl, for the discussions on the Minto Flats Seismic zone and Interior Seismicity. And for the classes that taught me about seismology, geophysics, and how to solve a problem.

Helena Buurman provided many conversations about both of the projects, and her help was invaluable. Celso Alvizuri also provided good insights and helped me to interpret the processes occurring at Uturuncu. And to the rest of the tea group, including Taryn Lopez, Dara Merz, Stefanie Whittaker, Tim Bartholomaus, and Kathleen McKee, thank you.

There are numerous friends that made my time in Fairbanks some of the best I could imagine. There are too many to list.

I probably would not have made it to this point without the constant support of my family, so thank you for everything you have done or said or that look you've given that makes me go, "Of course I can do it!"

And lastly, my wife Diana made sure that I ate when stressed, laughed when down, worked when I needed to, and made all of this so much better than it possibly could have been otherwise.

Introduction

Earthquakes can be powerful enough to destroy cities or so small that nobody feels them. They can occur where continents collide, deep in subduction zones, in the middle of the continent, around volcanoes, and elsewhere. Regardless of the size or environment, they all share something in common: earthquakes are the crust's brittle response to stress. This has two implications.

First, where one earthquake occurs, others will likely occur at some point in the future. If we know where earthquakes have occurred in the past, we can predict where they may occur in the future. As well, we can learn something of the seismic hazard associated with the faults that produce them. A fault that can produce an M8 earthquake is much more hazardous than one that is capable only of producing an M3 or less. It is important to have an accurate sense of the seismic hazard of a region for building codes, public safety, and particularly in Alaska, petroleum development and infrastructure.

Second, we can use seismic data to determine the stress pattern of a region. We might want to do this to better understand the tectonic setting, or as in the case of this project, determine the stresses at play in a volcanic setting. Seismicity is one of the key tools that scientists use to monitor volcanoes, as it is one of the few ways that we can track the processes occurring within and below the volcano.

By using earthquake locations, we can map out the faults and cracks on which they occur. We then interpret the geology, processes, and hazards associated with the seismicity from those patterns. But interpretations rely on accurate earthquake locations. Location errors can be on the order of kilometers. If we would like to talk about structures that are also on the order of kilometers, we must improve the earthquake locations. In order to reduce the relative location error, we relocate the earthquakes relative to each other.

This thesis consists of two study regions, tied together through a common goal and methodology. I spend Chapter 1 discussing the particular methods we use to both relocate the earthquakes and to group similar-looking earthquakes into families.

In Chapter 2, I discuss Uturuncu volcano in southern Bolivia where I aim to understand the source of stresses in the vicinity of the volcano by examining seismic patterns. InSAR data from the 1990s show that the volcano was inflating at a rate of 1-2 cm per year (Pritchard & Simons,

2002), which is a strong signal given that it has not erupted in over 270 ka (Sparks *et al.*, 2008). Uturuncu previously erupted in a series of very large ignimbrite eruptions and sits upon one of the largest magma bodies in the world (deSilva, 1989). The observed deformation signal prompted a cross-disciplinary group to begin studying the volcano. One of the fundamental questions is whether the earthquakes occurring there are due to regional or local volcanic stresses. If the earthquakes are volcanic, it could have implications for magma or fluid movement beneath the volcano, which in turn can improve our understanding of volcanic processes or pluton emplacement. By creating high precision relative relocations of the earthquakes around Uturuncu, I can begin to answer that question more reliably.

Chapter 3 focuses on Interior Alaska, a seismically active region that has few mapped faults with confirmed Holocene offset. I refine clouds of seismicity into lineaments that are then used to gain better understanding of both the extent of faulting and the mechanism driving deformation. One of the leading theories about the driving mechanism causing the seismicity in the Interior is block rotation by compression and shearing (Page *et al.*, 1995). I use high-precision earthquake relocations to examine the seismic patterns and interpret possible fault planes, which are used to support or negate this theory, as well as other competing ideas. I further delve into three specific faults that produced large earthquakes (M5-M6) within the Minto Flats Seismic Zone (MFSZ), west of Fairbanks. Despite being the longest of the seismic zones, with the potential to produce more large earthquakes, the MFSZ is relatively unstudied. By examining these three fault sequences, I am able to add to our knowledge of the region and tie it into the rest of the Interior.

Chapter 1 A Procedure to Calculate High-Precision Double-Difference Relocations

All methods used in this study begin with a pre-existing catalog of analyst-reviewed earthquakes. From those catalogs, we extract origin, travel time, and waveform data in order to produce cross-correlations and double-difference relocations. The particulars of each catalog (Uturuncu Volcano and Interior Alaska) are discussed later, in their respective chapters.

There are many terms used to describe a set of similar-looking earthquakes. These include "cluster," "family," "multiplet," occasionally "swarm," amongst others. Here, we use the term "family" to distinguish a cross-correlation grouping of events with similar waveforms from a "cluster" of interconnected events used during relocation. We do not intend to make a statement about the source of the earthquakes through this terminology, merely distinguish groups of similar-looking ones from the rest.

1.1 Families of Repeating Earthquakes – Cross Correlations

We use cross-correlations for two distinct purposes in these studies. The theory behind the procedure is the same in both cases, and as such we describe the particulars in more depth here, where we discuss families of similar-looking earthquakes. We leave out the details when we describe the application to double-difference later in this chapter.

The signal recorded by a seismometer is the convolution of the source-time function and radiation pattern emitted during the earthquake (source), the velocity and structure of the materials that the waves propagate through (path), and the response of the seismometer itself (receiver). Energy is reflected and refracted at every interface, which turns an otherwise simple waveform into the complex pattern we actually record. Each individual wiggle is affected by the structure of the medium traversed and, as such, changing the path will change the shape of the waveform.

We use cross-correlation to assess waveform similarity. This can be done in either the time domain or the frequency domain. In the time domain, correlations are a sliding convolution of two waveforms. By taking the Fourier transform to the frequency domain, the convolution becomes a multiplication, which is computationally more efficient to perform. Because every waveform is cross-correlated with every other earthquake, the number of cross-correlations

grows exponentially with the number of earthquakes. While it is time-consuming to convert from the time domain to the frequency domain, the increase in computational speed to execute large numbers of multiplications outweighs the time it takes to perform the conversion. For this reason, all correlations used here are calculated in the frequency domain.

During the cross-correlation process, two types of values are produced: correlation values and lag times. A correlation value is produced for every time step as the waveforms are shifted past each other. Only the largest correlation value (and corresponding lag time) is retained and used to describe the similarity of two waveforms. The correlation value, ranging from -1 to 1, is a measure of how similar the two waveforms are over the specified window. The lag time is the time shift required to align the two waveforms to achieve the maximum correlation value. We create sub-sample precision by interpolating the waveform between samples using a second-order polynomial fit.

An important consideration is the length of the waveforms to be cross-correlated – or, to be more precise, the number of cycles being cross-correlated. For high frequency waveforms, a shorter window is sufficient, while longer periods require a longer time window. A window of a few seconds is long enough to identify families reliably for the seismograms used in the Interior and Uturuncu studies. Such a long window is beneficial when studying repeating earthquakes and can ensure good correlation pairs, but limits the number of pairs with high correlation values. Shorter windows can provide larger numbers of high-correlation pairs but also increase the possibility of cycle skipping or poor overall similarity between the pair. When looking for similar events it is better to have a longer window, but in some cases (such as during relocation) it is better to increase the number of earthquake pairs. Therefore, it is important to have a grasp on the purpose of the cross-correlations before choosing the parameters that define it.

The frequency content of the waveforms necessarily affects their correlation value. It makes sense that two earthquakes consisting of different frequency contents will correlate poorly compared to events which share the same frequencies. In real data, there are often many sources of noise that affect the frequency content of the waveform. This includes both low frequencies, such as microseisms, and higher frequencies like wind noise. Two otherwise similar earthquakes may look different while being recorded due to these types of noise sources. In order to eliminate these sources of noise that might contaminate the data, we filter the waveforms. In

doing so, we help to ensure that two similar events do indeed correlate well. Too much filtering can make two dissimilar waveforms begin to look similar, though, and can generate artificially higher correlation values. For this reason, we avoid heavy filtering.

Due to the complexity of the waveform, two earthquakes that produce highly similar waveforms must originate nearby each other and have the same mechanism. As a rule of thumb, how sensitive a wave is to heterogeneities is dependent on the length scale of the heterogeneities and the frequency of the wave. Typically, waves are sensitive to structures larger than one quarter of the wavelength (Geller and Mueller, 1980). Similarly, waveforms from earthquakes within a quarter of the dominant wavelength of each other will be highly similar as long as they have the same rupture mechanism.

Repeating earthquakes can also have important implications for the source mechanism and improve our understanding of the processes at play. Additionally, it provides an independent way to determine the validity of earthquake locations and an improved understanding of the true errors associated in earthquake locations.

1.2 Double-difference Method

Spatial earthquake patterns can be a powerful tool for understanding the structure and mechanics of an actively deforming region, but the interpretation is only as good as the earthquake locations. By relocating the earthquakes using the double-difference method (Waldhauser & Ellsworth, 2000), we are able to improve the relative locations and therefore enhance the resolution of the structures that produce them.

Double-difference is one of a handful of methods that can be used to perform earthquake relocations. A similar method is the Joint Hypocentral Determination (JHD) method. During JHD multiple earthquake hypocenters are solved for at the same time, as well as a correction to the stations. Double-difference, on the other hand, does not solve for station corrections. It instead uses travel time differences of event pairs, which eliminates the need for such corrections.

Double-difference Relocation

The fundamental assumption underlying double-difference relocation is that differences in travel times for two earthquakes are due to a difference in source location, rather than a difference in velocity structure along the paths. This assumption is met only when the distance between the two earthquakes is small compared to the distance to a common recording station. For those events, the paths travelled by the waves are nearly identical and we assume that they travel through the same velocity structure.

Because we difference the travel times for the two earthquakes, many of the unknowns – including path and station unknowns that add errors to the location – are largely subtracted out (Waldhauser & Ellsworth, 2000). What remains is the travel time associated with the difference in path length between the two earthquakes and the station. By calculating the travel time differences for an event pair at many stations, it is possible to accurately determine the relative position of the two earthquakes.

The approach we use creates a web of connected event pairs, termed a cluster. This web is then located as a group such that all events are shifted relative to each other. By solving jointly for all solutions at once, earthquakes that are too far apart to relocate directly can be located relative to each other through a chain of other earthquakes. It also means that all of the earthquakes within a cluster affect the locations of all other earthquakes within that cluster.

Since the relocation process uses travel time difference to calculate spatial shifts, the key data used are travel times. We use travel times for both the P and S phases. While all data are travel times, there are two types of travel time data used: catalog and cross-correlation travel times.

Catalog Travel Times

"Catalog travel times" are the time it takes for energy to travel from the origin to the recording station, as measured by the phase picks in the earthquake catalog. Catalog data is therefore the difference in the catalog travel times for an event pair to a common station. This value can be calculated for every event pair that is recorded at a common station, regardless of the distance between the two earthquakes. Because of this, catalog data are available for all pairs that we include during relocation. While using catalog data does improve the relative locations,

erroneous or inconsistent picks can affect the calculated travel times, which are then translated into errors in the locations. We can improve the accuracy of the relative pick times, which in turn improves the differential travel time.

Cross-correlation Travel Times

Cross-correlation provides a way to correct for inconsistencies in picked arrival times. As described previously, all waveforms are filtered to remove noise prior to correlation. For event pairs that produce similar arrivals, we calculate the cross-correlation lag time between the two. Unlike cross-correlations for the purpose of generating families, here we are more concerned with aligning the initial arrivals (for both P and S) than in ensuring event similarity. The time frame is chosen in order to allow multiple cycles in the waveform, but preferably not too many as we want to align only the very initial arrival. Hypothetically this can be done using just the first pulse of energy, but since many waveforms are noisy or may be poorly picked, we expand the window before and after the picked arrival. As long as there is similarity in the arrival – the same polarity and similar frequency content – we are able to produce a better alignment of the two arrivals by adding the lag time to the catalog travel time difference. We use this time correction only for those pairs that correlate at 0.7 or greater. This is because, as mentioned, a lag time is produced no matter how similar or different the waveforms may be and we want to keep only those lag times that are meaningful.

The corrected travel time difference is used as an independent dataset, cross-correlation differential travel times. This corrected dataset produces higher precision relocations, but the data is not available for all event pairs and we must rely on a combination of both catalog and cross-correlation data.

Work Flow

To get relocations from catalog data, there are three important steps that must be taken, each with their own set of parameters that must be optimized for the particular dataset (Figure 1.1).

First, pre-processing pairs earthquakes based on a series of distance thresholds and observation requirements. This is done in order to pair well-connected earthquakes and discard

those that would destabilize the relocation process. To do this pairing, we use the program ph2dt (Waldhauser, 2012). Here, "well-connected" implies two things: 1) since the core data are travel time differences, both earthquakes of a pair must be recorded at many common stations and 2) that any given earthquake is paired to multiple other earthquakes. The exact number to define what is well-connected depends on the study, but the number of paired earthquakes should be large enough to allow the system to be solved, but not so large as to computationally overwhelm the computer. Here we use a minimum of 8 shared stations to define a pair and require a minimum of 8 pairs for an event to be included during relocation. In regard to distances, it is important that the assumption at the very basis of double-difference is met and that the paired earthquakes are located nearby each other relative to the distances to the stations. The maximum distance between paired events is a user-defined value, which will depend on the density of earthquakes in the dataset and the distance to the stations recording them. A region with sparse seismicity may require a greater minimum distance threshold so that enough earthquakes can be paired to perform the relocation. Similarly, if the network used to record the seismicity is spread across a larger region, a greater distance threshold can be used than if it is a small network.

Because we use cross-correlation data, the next step is to calculate the lag time for each of the previously selected event pairs. There are few parameters during this step – correlation window, filter, and minimum correlation value - but they are quite important to the amount of cross-correlation differential times produced. As described previously, a smaller window may produce more earthquake pairs that meet the minimum correlation value, whereas a longer window will produce fewer.

Finally, to perform the double-difference relocations we use hypoDD2.1b (Waldhauser, 2012). The outputs from the previous two steps are input, as well as an array of other parameters. A number of the parameters simply define the way in which the program will solve the problem: the mathematical method to be used, whether earthquakes locating in the air should be discarded, and where to place earthquake origins to begin the relocation process, to name a few. There is also a set of parameters that nearly duplicated those used during clustering, including the minimum number of observations required to define a pair and the minimum or maximum distance between the pair and stations. These are meant to allow for greater restriction during relocation than during clustering. Finally, relocation is an iterative process and during

each step the partial derivatives are calculated and the origins are shifted accordingly. Each iteration has a set of parameters that are used to weight the data, discard outliers, and damp the inversion.

Sensitivity Tests

All datasets used for these projects are large enough that we must use a Least-Squares QR (LSQR) method to solve the inverse problem at the core of the relocation. While this is more efficient for large datasets, it does a poor job at estimating the error associated with the relocations (Waldhauser & Ellsworth, 2000). In order to get an idea of how stable the results are, we perform a series of sensitivity tests. We test the sensitivity for stations, events, and velocity model. Because events are tied together and relocated relative to each other through shared observations, the particular stations used during relocation can affect the results. Similarly, the individual earthquakes included in the process have an effect on the final locations of the other earthquakes. Finally, perhaps most obvious, the velocity model can have a very large affect on the final locations, and it is important to get a sense of how stable the structures are regardless of velocity model used.

We perform Jackknife tests, wherein we remove a single station or event and relocate the remaining data. This is done for all stations and all earthquakes such that any given run is missing a single station or single earthquake. Each run will produce slightly different final locations. How different the locations are will depend on the dataset, station orientation, and stability of the relocation.

To distill the distribution into a simple set of numbers, we calculate the variance of the distribution in earthquake location. For each earthquake, the mean X, Y, and Z position is calculated. We then calculate the difference from each "final location" produced during the Jackknife tests to the mean position for that earthquake (dX, dY, and dZ). This is done for every earthquake, producing a large set of dX, dY, and dZ values. We calculate the standard deviation of each dX, dY, and dZ to get an idea of the magnitude and direction of error associated with the tests we performed.

The velocity tests are not Jackknife tests but are used instead to ensure that the observed structures are relatively stable regardless of velocity. There is less meaning associated with the

positional shifts of the velocity, and as such we do not calculate the standard deviations for the velocity tests.

1.3 References

Geller, R. J., and C.S. Mueller (1980), Four similar earthquakes in central California, *Geophys. Res. Lett.,* 7, 821-824.

Waldhauser, F. (2012), HypoDD version 2.1b A Program to Compute Double-Difference Hypocenter Locations.

Waldhauser, F., and W. L. Ellsworth (2000), A Double-Difference Earthquake Location Algorithm: Method and Application to the Northern Hayward Fault, California, *Bulletin of the Seismolgical Society of America*, *90*(6), 1353-1368.

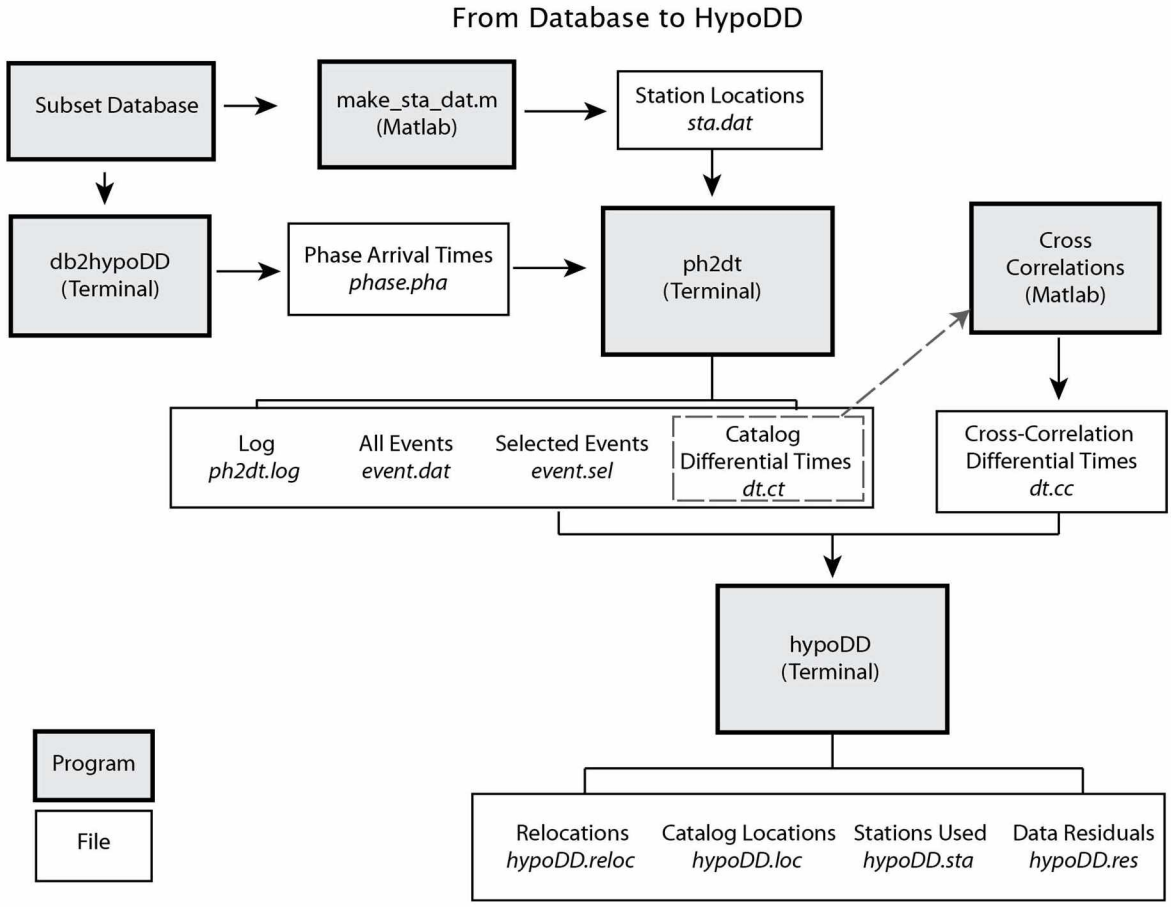

Figure 1.1 Flow chart of the process used during relocation.

Chapter 2 . Double-Difference Relocation of Earthquakes at Uturuncu Volcano, Bolivia [1]

2.1 Introduction

Uturuncu, located in southern Bolivia near the Chile and Argentina border (Figure 2.1), is a dacitic volcano that was last active around 270 ka (Sparks *et al.*, 2008). It is a part of the Altiplano-Puna Volcanic Complex (APVC), a large volcanic region that spans 50,000 km^2 between 21°S and 24°S(deSilva, 1989). The APVC is characterized by a series of ignimbrite flare-ups since ~23 Ma, originating from several large caldera complexes (deSilva, 1989). Multiple sets of evidence suggest that the region is underlain by a large magma body, which generated the source of eruptions.

First, seismic evidence shows that there is a low velocity layer, consistent with a magmatic body. Depending on the study, the depth extent varies from just under a kilometer thick located around 19 km below the surface (Chmielowski *et al.*, 1999) to nearly 20 km thick starting at 10 km beneath the surface (Ward *et al.*, 2014). The difference between those values is due to differences in methods, which have differing sensitivities. Chmielowski *et al.* (1999), using teleseismic receiver functions, found a pervasive 2 s negative-polarity P-to-S conversion that they modeled as the top of a low velocity layer at 19 km. Ward *et al.* (2014) used joint receiver functions and Rayleigh wave dispersion in their study. Their results suggest that the Altiplano-Puna Magma Body is much thicker, ranging from ~5 km below sea level to 25 km below sea level, with up to 25% melt present.

In addition, Schilling *et al.* (1997) used magnetotelluric and geomagnetic deep soundings to show that there is high electrical conductivity between 10 km and 30 km. In that study, the anomalously high conductivity is interpreted as partial melt, for which they calculate a range of 14-27% melt volume. This magma body, the so called Altiplano-Puna Magma Body, or APMB, is likely the source of the volcanic activity in the region. Based on the chemical consistency of the eruptive products, both spatially and temporally, the dacitic melt is thought to be due to crustal thickening – it occurs in a region of very thick continental crust, up to around 70 km – rather than melt associated with the subducting oceanic plate below (deSilva, 1989).

[1] Hutchinson, L.K., M.E. West, anC. Alvizuri, 2015. Double-Difference Relocation of Earthquakes at Uturuncu Volcano, Bolivia. Prepared for submission in *Seismological Research Letters.*

Although Uturuncu has not erupted in 270 thousand years, InSAR studies show that during the 1990s, the volcano experienced an average uplift of about 1 to 2 cm per year, consistent with an expanding source at 15-17 km depth (Pritchard and Simons, 2002).

In addition to the observed deformation at the volcano, there are identified faults in the proximity of Uturuncu that strike roughly northwest (Norini *et al.*, 2013); (Riller *et al.*, 2001) . One of the fundamental questions is whether the seismicity recorded at Uturuncu is associated with the regional stresses or whether they are a product of activity at the volcano. The aim of this study is to answer that question and add some insight into the processes occurring at Uturuncu and in the APMB as a whole.

2.2 Earthquakes

This study utilizes a dataset that was acquired using a temporary deployment of a total of 33 seismometers between April 2010 and October 2012. Using Guralp CMG 3T (120s) seismometers, we deployed an array that surrounded the volcano with a grid spacing of 10-20 km and a 100 km aperture (Figure 2.1). Seismometers had direct burials and data were stored on RefTek RT130s. Because of the international customs regulations, instruments were deployed and retrieved in a rolling fashion, such that no instrument was in place for more than 2 years. This means that no seismometer was in place for the entire length of the study.

Due to the remote location of the volcano, data were stored and collected in six-month increments when field crews visited and serviced the sites. Waveforms were then scanned using an automated program that selected a set of potential phase detections based on a short-term average to long-term average criterion. When phase detections from several stations clustered tightly in time, they were compared to the travel times from a pre-computed grid of hypocenters across the region. If the assemblage of detections matched the expected move out for a hypocenter within the grid, the event was added to the earthquake catalog and the hypocenter was set as the best-fitting grid point. Each earthquake in this draft catalog was examined by an analyst and the picks were refined. More picks, including S arrivals and arrivals on other stations, if distinguishable, were added to the earthquake solution and it was located again. Regional and teleseismic earthquakes are not included in the catalog as they are not of interest for this study. In some cases regional earthquakes manage to make their way into the catalog,

but they tend to locate at the edge of the search grid and have a poor fit to the data. Table 1.1 has the velocity model used during the location process.

This project focuses on 592 recorded earthquakes that occurred between April 2010 and March 2012 (Figure 2.2a). These earthquakes have over 5200 P phases (an average of over 8 per earthquake) and over 3400 picked S phases (over 5 per earthquake). Magnitudes range between M_L -0.65 to M_L 3.33 with a magnitude of completeness, Mc, of approximately 0.25. The magnitude of completeness varies with location: within the array there is an Mc -0.1 and a b-value of 0.8, whereas outside of the array Mc is closer to 0.7 with a b-value of 0.7 (Figure 2.3). These b-values are relatively close and are within error of each other. Higher b-values indicate a relatively greater portion of small events relative to large ones, while lower b-values mean that there are more large events to small ones. The magnitude distribution indicates the amount of stress capable of building up before a fault ruptures. If relatively more large earthquakes occur, there is a greater stress buildup. The world average for b-value is ~1, and the low value here might indicate that the earthquakes are likely more tectonic in origin. Because earthquakes outside of the array have poorer locations and a higher magnitude of completeness than those within, I include all earthquakes in the analysis but focus primarily on earthquakes within the array.

Depths are relative to the surface unless otherwise noted. The primary reason for converting from a sea level baseline to a surface baseline is that hypoDD, the program used to relocate the earthquakes, is unable to locate above the zero reference level. Here there is a 4-5 km difference between sea level and the surface – a region that produces earthquakes that need to be relocated. We use the elevation of the lowest station, or 4.085 km, as the surface.

There are two depths where we observe bands of seismicity in the catalog. The first is a strong layer of seismicity at ~10 km below the surface. The original velocity model (Table 2.1) has a velocity layer boundary at that depth; both a higher-than-reality velocity of the upper layer and/or a slower-than-reality velocity in the lower layer would shift earthquakes to the boundary as long as there is a sufficient contrast in velocity of the two layers. But, while the concentration at 10 km is suspicious, it does not rule out the possibility of an increase in seismicity at these shallower depths. Second, there is a light layer of seismicity, with no earthquakes occurring above it, at 3 km above sea level (1 km below the surface). This boundary is a product of the

original location algorithm, which did not locate any earthquakes shallower than 3 km above sea level. Because we locate earthquakes using a grid search to minimize the misfit, we would expect shallower earthquakes to locate near the upper boundary - the relative lack of earthquakes that abut the 3.0 km boundary indicate that this was not a major issue. We use a different velocity model during relocation, with different velocity boundaries. As such, the patterns will only persist if they are real. Otherwise, the earthquakes should shift to their proper relative locations.

Based on observations, we categorized the earthquakes into three primary types of signals: local earthquakes, long period earthquakes, and mining blasts (Figure 2.4).

Local Earthquakes

The majority of earthquakes in the catalog are "typical" earthquakes with clean and distinct P and S arrivals. Volcano-tectonic (VT) earthquakes are caused by the mechanical breaking of brittle rock, such as slip on a fault or the fracture at a tip of a dike (e.g. McNutt, 2002). Despite the volcanic environment, there is a distinct lack of typical low frequency earthquakes (LFEs) that indicate fluid movement (e.g. Aki *et al.*, 1977; Chouet, 1981; Chouet, 1988; Crosson and Bame, 1985). This is in contrast to nearby Lastarria volcano, in Chile, which shows monochromatic, gradual onset LFEs. The absence of these earthquakes does not mean that there are no fluids flowing below the surface. Moment tensor analysis on a subset of larger earthquakes indicates that there are a variety of earthquake sources; some fit the opening or closing of a volume while others fit a double-couple model better (Alvizuri and Tape, 2014). The lack of low-frequency events merely indicates that they did not produce dominantly long period energy.

Long Period Earthquakes

There are events, albeit far less common, that do have a dominant long period signal. They do not quite look like LFEs, but it is difficult to distinguish whether their low frequency content is due to source or path effects. It seems that the high frequency energy has been stripped away, leaving a dominantly low-frequency signal. In addition, the majority of the S-wave energy is missing. They differ from the typical volcanic LFE in that they have a more abrupt onset and are

less monochromatic. This is consistent with waves travelling through a melt-rich layer such as the APMB where attenuation would be high and shear motion is damped or eliminated altogether. The majority of the deep earthquakes (>30 km) are recorded as these long period signals. In addition, there are shallower earthquakes that look similar and could indicate the presence of melt at shallower depths. On the other hand, they could be hybrid earthquakes formed by fluid flow. While it is difficult to distinguish whether they are hybrid earthquakes or have been attenuated, we are inclined to interpret them as the latter. For these earthquakes, it seems more likely that the missing frequencies are due to attenuation rather than a fluid-generated source.

Mining Blasts

The third type of event recorded during this time is mining blasts. The region to the southeast of the array hosts many of these mining events. They are recognizable by the relatively high amplitude P arrival and a long, low-frequency coda that follows the initial high-frequency energy (e.g. Beck and Wallace, 1995; Yilmaz *et al.*, 2012). In some ways, they look visibly similar to the long period events, but they include a distinct S-wave arrival and contain more high-frequency energy in both the P and S arrivals. Another strong indicator for the mining origin of these earthquakes is their distinct time of occurrence in the day. While these events are recorded over the entire time span of the study, they occur within the same 5 hours of the day, indicating that they are not a naturally occurring phenomenon (figure 2.5). The primary set of these mining blasts occurs outside, and southeast, of the array leading to poorly constrained locations. Location errors are compounded by the fact that there are relatively few S picks on the mining events. Without S-P times to constrain the distance from the source to receiver, the locations are much less reliable. Because of the location challenges, along with their anthropogenic origin, we have removed them from our analysis.

2.3 Results

Families of Similar Earthquakes

We performed cross-correlations for all earthquakes within the array, using phases recorded at all stations. The exact pairs that correlate well will vary depending on the particular

station used during correlation, but overall groupings are persistent regardless of the station used in analysis. Here, we use station PLSE because it recorded the largest number of high-correlation earthquake pairs. We apply a bandpass filter of 1-15 Hz to eliminate longer period noise that can artificially dominate the correlation. We use a correlation window of 4.5 seconds, from 1 second prior to the arrival until 3.5 seconds after, and a minimum correlation value of 0.7. This is long enough to ensure that high correlation values truly indicate similar waveforms.

There are 7 families with 5 or more earthquakes, for a total of 61 earthquakes that fall into the 12 largest families (Figure 2.6). Some of these families, such as 2 and 9, or 4 and 8, are likely related but are just dissimilar enough to fall below the 0.7 correlation value threshold. This is confirmed by the similar timing of families 2, 4, and 9. In addition, there are earthquakes that locate amongst a family but do not fall within that family. These are probably also related to the nearby family but are either just dissimilar enough to be cut from the family or were not recorded at station PLSE. The earthquakes in each family have a tendency to cluster tightly and are generally distributed along a radial pattern centered just south of the summit (Figure 2.7). The tight clustering is expected, as earthquakes that have similar waveforms must locate nearby one another, but the radial pattern may be suggestive of the stress field near the volcano.

We fit a plane to each family of earthquakes to get a quantitative value for the orientation of the potential fault planes (Figure 2.7). This is done by using a least-squares fit to the data, with outliers removed. In some cases, there were earthquakes that clustered nearby each other but were not a part of the same family when using PLSE. I include these earthquakes when calculating the best-fit plane. Additionally, I combine nearby families (such as 2 and 9) for the fit because they all fall together as part of one linear structure. All planes are fit to the double-difference locations (discussed below), rather than the catalog data.

Double-difference Relocations

Of the original 592 earthquakes in the catalog - with mining blasts removed – 413 meet the criteria for relocation (Figure 2.8; Figure 2.9). For earthquakes to be paired during pre-processing, we require a maximum separation in the original catalog locations of no more than 10 km and a minimum of eight common phase arrivals (same phase, same station). We err on the side of liberal pairing. It is possible to further restrict these criteria again during the

relocation inversion. We use both catalog and cross-correlation data for P and S arrivals. A minimum of 12 observations are required to define a cluster during relocation. Cross-correlation data is calculated for both P and S arrivals using a 1 second window from 0.25 s before the pick until 0.75 s after and we apply a bandpass 1-15 Hz filter. In order for the correlation data to be used, the waveforms have to correlate at a minimum of 0.7 over that window.

Figure 2.10 shows the results of the relocations. Directly around the volcano, the most noticeable difference occurs where many of the earthquake clusters have pulled together more tightly. In map view, there is a relatively dense population of earthquakes in the region of greatest uplift. In cross-sectional view (Figure 2.10b), we see that they fall within a convex upward distribution, centered beneath the summit. Earthquakes have shifted upward from the original catalog locations, but still maintain a strong banding at depth. This band sits at approximately 5-10 km below the surface and spans around 10 km laterally, centered just south of the volcano.

Outside of the array, there is limited change in earthquake locations when comparing the relocated earthquakes to the original catalog. This is not surprising, given the decrease in earthquake density in that region. Each earthquake is less well connected with other earthquakes, and most relocation clusters tend to include just a single pair of events. While this improves the relative location of those two earthquakes, it does little to improve the location of the pair relative to the rest of the seismicity.

Sensitivity Tests

The results of the sensitivity tests can be seen in Figure 2.11 and Figure 2.12. The standard deviations (σ) of earthquake locations for the event sensitivity test are less than 150 m, and the station tests have a σ of less than 1 km (Table 2.2). The higher values for the station tests indicate that there is a greater dependence on the particular stations used during relocation than on the particular events included. Figure 2.12 shows that most earthquakes have stable locations, but there are some that are problematic – they likely skew the σ value upward.

2.4 Discussion

There are two possible sources of the stresses that produced the seismicity recorded on the array around Uturuncu: regional stresses and local stresses. First, there are a series of NW-

striking faults that run through the Altiplano and Chile, including the left-lateral Lipez-Coranzuli fault system that runs through southern Bolivia near Uturuncu Volcano (Figure 2.13). Those faults are expressions of the tectonic stresses present throughout the region, caused by subduction of the Nazca plate, which is thought to be a primary factor in the volcanic pattern of the region (Riller *et al.*, 2001). Additionally, we know that the volcano has experienced uplift centered on the summit (Pritchard and Simons, 2002). There could be stresses related directly to the uplift as well as stresses related to fluid flow underneath the volcano (which could be part of the cause of inflation in the first place). The goal is to use the earthquake patterns to try to improve our understanding of the stresses at play at Uturuncu.

2.4.1 Families of Similar Earthquakes

The fact that there are repeating earthquakes - some families short-lived, some lasting through years - means that there must be a relatively non-destructive, repetitive source. Because it requires the same source mechanism to produce similar waveforms, we know that the same type of fracturing occurred repeatedly. For example, either slip along a well-defined fault or the progressive opening of a crack could produce long-lived, repeated seismicity.

In addition to knowing that the source is repetitive, the vast majority of the repeating earthquakes outline planar or linear features. Therefore, we know that the earthquakes are occurring on fault planes or cracks. For our purposes here, the difference between a fault and a crack is whether the earthquake motions are double-couple or not, respectively. Based purely on earthquake locations, it is very difficult to distinguish slip parallel to a fault from fracturing perpendicular to a crack. This is especially so given the lack of low frequency earthquakes that might otherwise be suggestive of volume change and/or fluid flow.

Alvizuri and Tape (2014) calculate first-motion and full-body waveform focal mechanisms for the largest earthquakes in the catalog. Of the families we identify, a handful include events that they examined. Because repeating earthquakes must have a similar mechanism, we can assume that other earthquakes within the same family have the same, or very similar, moment tensor, or at least similar stress axes. Interestingly, while a few events have predominantly double-couple motion, the majority of the earthquakes large enough for moment tensor analysis have a significant component of non-double-couple motion (Figure 2.7). They could correspond

to the opening of a dike or pipe, as most show a positive isotropic component. The most likely cause of these motions, in the context of Uturuncu, is a component of fluid or gas movement. In fact, there are a number of earthquakes that show entirely outward motion – all stations record the same positive first motion P waves. This is observed for events well within the array and with good station coverage. It is not possible to say with certainty that such events are not the opening of an optimally-oriented crack, rather than a purely explosive source, but it is possible to discount double-couple motion for those events.

For those families and related families for which we have more than one moment tensor, we see that there are occasionally both predominantly double-couple and non-double-couple earthquakes in close proximity to each other. We suggest that this shows that there are multiple processes occurring at the cracks. Some earthquakes demonstrate a greater component of double-couple than others. The two of these events that occur as a part of family 2 show dextral strike-slip motion with a nearly horizontal NNW maximum stress axis. The motion is opposite of the regional strike-slip faults but aligns nearly perfectly with the expected stress pattern from Uturuncu's inflation (Figure 2.7). Perhaps the earthquakes represent different parts of the same process. The double-couple earthquakes are caused by increased stress as fluids move toward a region, resulting in the readjustment along faults prior to the actual arrival and passage of the fluids. As the fluid reaches and moves through the same region, it would show increased non-double-couple motion caused by the fluids moving through the crack.

Independent of seismic data and interpretations, there is another indicator of fluid flow at the volcano: Uturuncu has active sulfurous fumaroles. The sulfurous component to the gases strongly suggests a magmatic source, regardless of whether there is a meteoric component as well. Many of the earthquakes occur at 5-10 km below the surface; while it is possible for water to be moving through the crust at those depths, it is a bit deep for a well-developed meteoric system. This suggests that the fluids causing the earthquakes are largely magmatic in source.

Regardless of the particular fluid causing the earthquakes, the pattern of the orientation of the cracks can give us insight into the stress pattern near the volcano. A fluid-filled crack will propagate in the direction of the maximum compressive stress (Scholz, 2002), thus we can use the orientation of the fitted planes as a proxy for the maximum compressive stress. Given the repeating nature of the families and the moment tensors that we do have, we assume that the

earthquakes that occur in families are due to fluid flow even if we do not have moment tensors for that particular family. The pattern we observe seems to be due to neither fully regional nor fully local stresses.

The regional strike-slip faults suggest that the regional stresses are relatively uniform over a large region, much larger than the area of our study. If the earthquakes were due to purely regional stresses, we would expect a series of nearly parallel cracks. Given the orientation of the left-lateral strike-slip faults (Riller *et al.,* 2001), maximum compressive stress is likely roughly E-W (in agreement with the general direction of convergence at the plate boundary). This would generate a series of E-W striking faults, which is not what we observe. Particularly to the north and south of the volcano, families of earthquakes are oriented far from E-W.

Local volcanic stresses are expected to produce a radial pattern. The horizontal stresses associated with an inflating source at depth are radially outward from the source (Mogi, 1958). While this is similar to what we observe, the pattern is far from purely radial. Again, the regions to the north and south, in particular, stray from this pattern.

We suggest that we see an overprinting of local stresses on a background of regional stresses. To the east and west of Uturuncu, the local and regional stress directions roughly align, producing E-W oriented cracks. The further north or south the family is, the more there is a balance between local and regional stresses. The particular orientation of the cracks will depend on the magnitude of the stresses and how they sum together. Together, the stresses should combine to produce a field that is somewhere between the two end members, producing crack orientations somewhere between the two expected directions. This is indeed what we observe.

2.4.2 Overall Seismic Patterns

With the removal of the mining events from the catalog, the previously noted, broad NW-SE pattern (Jay *et al.*, 2011) is much harder to observe. The particular earthquakes recorded during this time seem to suggest that directly around the volcano, local volcanic stresses play an important role in determining earthquake occurrence and orientation. But, as we note from the families of repeating earthquakes, shear stresses are present in the crust, and the lack of an overall NW-SE pattern to the seismicity does not eliminate the probability that shearing plays a

role in the weaknesses of the crust and overall seismic and volcanic patterns of the APVC (Riller *et al.*, 2001).

Perhaps the most noticeable pattern is the convex upward layer of seismicity at 10 km beneath Uturuncu (Figure 2.10c, d). A very similar layer was previously recorded during a temporary deployment of seismometers in 2009-2010 and attributed to the top of the brittle-ductile transition (Jay *et al.*, 2011). Subsequently, Ward *et al.* (2014) used joint Rayleigh wave dispersion and receiver functions to image a low S-velocity layer, interpreted as the APMB, from 10-30 km below the surface. They acknowledge that their method is not sensitive to narrow vertical structures and is therefore not at odds with high-resolution Bouguer anomaly modeling that shows a series of vertical, elongate low-density features that have been interpreted as diapiric magma bodies (del Potro *et al.*, 2013). Fialko and Pearse (2012) also suggests diapiric magma movement as the key mode of magma transport at the APMB, noting that the 'sombrero' pattern to surface deformation (i.e., uplift in the center surrounded by a moat of subsidence) is best explained by the pooling of magma at the top of the APMB as it begins to ascend. One such body correlates with the ground deformation and thermal anomalies associated with Uturuncu (del Potro *et al.*, 2013). West *et al.* (2013) used seismic tomography to find a deep, low velocity tabular body under Uturuncu, centered just south of the summit. We suggest that the seismicity we record is associated with the top of one of these diapirs, or fingers, of the APMB (Figure 2.14).

Two things are of note: 1) the band of seismicity at 5-10 km is isolated to directly underneath Uturuncu, and 2) there is seismicity at depths greater than 10 km further from the volcano. Together, these support the notion of a diapir rising up beneath Uturuncu. As the deep inflation applies stress to the shallow crust, the cap of brittle material expands upward and outward, reducing the compressive stress and allowing for fluid to move through the cracks. Below this layer, the rock is too hot for brittle deformation and fluid flow will be aseismic. The depth to the brittle-ductile transition at the volcano is dependent on the depth to which the diapir rises. Outside of this region, though, the brittle-ductile transition is deeper. This pattern supports the possibility of elongate, vertical bodies rising from the APMB, which would produce a heterogeneous temperature field and therefore a heterogeneous depth to the brittle-ductile transition.

2.5 Conclusions

The seismic patterns indicate two things. 1) There is a radial pattern to the stress field around Uturuncu volcano. The families of repeating earthquakes, which are largely non-double-couple and are likely formed from fluid flow through cracks or dikes, demonstrate a radial pattern that suggests that the maximum compressive stress is laterally outward from the volcano. This is consistent with the stress pattern expected from uplift caused by an inflating source at depth. 2) The layer of increased seismicity at 10 km depth is indicative of the brittle-ductile transition below Uturuncu, but deeper seismicity elsewhere suggests that the depth to this transition is heterogeneous. In addition, the lack of seismicity beneath the 10 km band at Uturuncu supports the possibility of a diapir rising beneath the volcano, which may be the source of past eruptions.

2.6 References cited

Aki, K., M. Fehler, and S. Das (1977), Source mechanism of volcanic tremor: fluid-driven crack models and their application to the 1963 kilauea eruption, *Journal of Volcanology and Geothermal Research*, *2*(3), 259287.

Alvizuri, C., and C. Tape (2014), Full Moment Tensors for Small (Mw<3) Events at Uturuncu Volcano, Bolivia, in *Seismological Society of America Annual Meeting*, edited, Anchorage, AK.

Beck, S. L., and T. C. Wallace (1995), Broadband Seismic Recordings of Mining Explosions and Earthquakes in South America, in *17th Seismic Research Symposium on Monitoring a CTBT*, edited, pp. 157-163, Scottsdale.

Chmielowski, J., G. Zandt, and C. Haberland (1999), The Central Andean Altiplano-Puna Magma Body, *Geophysical Research Letters*, *26*(6), 783-786.

Chouet, B. (1981), Ground motion in the near field of a fluid-driven crack and its interpretation in the study of shallow volcanic tremor, *Journal of Geophysical Research: Solid Earth (1978–2012)*, *86*(B7), 5985-6016.

Chouet, B. (1988), Resonance of a fluid-driven crack: Radiation properties and implications for the source of long-period events and harmonic tremor, *Journal of Geophysical Research: Solid Earth (1978–2012)*, *93*(B5), 4375-4400.

Crosson, R. S., and D. A. Bame (1985), A spherical source model for low frequency volcanic earthquakes, *Journal of Geophysical Research: Solid Earth (1978–2012)*, *90*(B12), 10237-10247.

del Potro, R., M. Diez, J. Blundy, and A. G. Camacho (2013), Diapiric ascent of silicic magma beneath the Bolivian Altiplano, *Geophysical Research Letters*, *40*(10), 2044-2048.

de Silva, S. L. (1989), Altiplano-Puna volcanic complex of the central Andes, *Geology*, *17*, 1102-1106.

Fialko, Y., and J. Pearse (2012), Sombrero uplift above the Altiplano-Puna Magma Body: evidence of a ballooning mid-crustal diapir, *Science (New York, N.Y.)*, *338*(6104), 250-252.

Jay, J. A., M. E. Pritchard, M. E. West, D. Christensen, M. Haney, E. Minaya, M. C. Sunagua, S. R. McNutt, and M. Zabala (2011), Shallow seismicity, triggered seismicity, and ambient noise tomography at the long-dormant Uturuncu Volcano, Bolivia, *Bulletin of Volcanology*, *74*(4), 817-837.

McNutt, S. R. (2002), Volcano Seismology and Monitoring for Eruptions, in *International handbook of earthquake and engineering seismology*, edited by W. H. K. Kanamori, P. C. Jennings and C. Kisslinger, Academic Press.

Mogi, K. (1958), Relations between the eruptions of various volcanoes and the deformations of the ground surface around them, Bull. Earthquake Res. Inst. Univ. Tokyo, 36, 99 – 134.

Norini, G., W. Baez, R. Becchio, J. Viramonte, G. Giordano, M. Arnosio, A. Pinton, and G. Groppelli (2013), The Calama–Olacapato–El Toro fault system in the Puna Plateau, Central Andes: Geodynamic implications and stratovolcanoes emplacement, *Tectonophysics*, *608*, 1280-1297.

Pritchard, M. E., and M. Simons (2002), A satellite geodetic survey of large-scale deformation of volcanic centres in the central Andes, *Nature*, *418*(6894), 167-171.

Riller, U., I. Petrinovic, J. Ramelow, M. Strecker, and O. Oncken (2001), Late Cenozoic tectonism, collapse caldera and plateau formation in the central Andes, *Earth and Planetary Science Letters*, *188*(3-4), 299311.

Schilling, F., G. Partzsch, H. Brasse, and G. Schwarz (1997), Partial melting below the magmatic arc in the central Andes deduced from geoelectromagnetic field experiments and laborator data, *Phys Earth Planet Inter*, *103*, 17-31.

Scholz, C. H. (2002), *The Mechanics of Earthquakes and Faulting*, Cambridge, UK, Cambridge University Press.

Sparks, R. S. J., C. B. Folkes, M. C. S. Humphreys, D. N. Barford, J. Clavero, M. C. Sunagua, S. R. McNutt, and M. E. Pritchard (2008), Uturuncu volcano, Bolivia: Volcanic unrest due to mid-crustal magma intrusion, *American Journal of Science*, *308*(6), 727-769.

Ward, K. M., G. Zandt, S. L. Beck, D. H. Christensen, and H. McFarlin (2014), Seismic imaging of the magmatic underpinnings beneath the Altiplano-Puna volcanic complex from the joint inversion of surface wave dispersion and receiver functions, *Earth and Planetary Science Letters*, *404*, 4353.

West, M. E., E. Kukarina, and I. Koulakov (2013), Structure of Uturuncu Volcano from Seismic Tomography, *American Geophysical Union Fall Meeting 2013*, San Francisco, CA.

Yilmaz, S., Y. Bayrak, and H. Cinar (2012), Discrimination of earthquakes and quarry blasts in the eastern Black Sea region of Turkey, *Journal of Seismology*, *17*(2), 721-734.

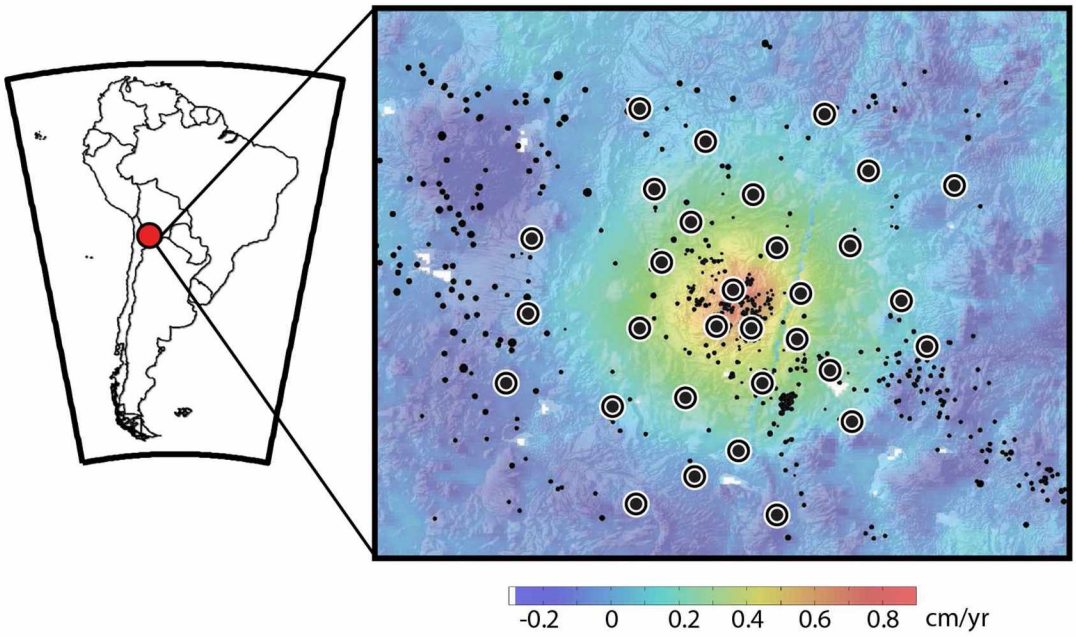

Figure 2.1 Regional map of Uturuncu.
Uturuncu Volcano, located in Southern Bolivia, is a part of the Altiplano-Puna Volcanic Complex, which is sourced from the Altiplano-Puna Magma Body. InSAR data from S. Henderson (personal communication, Nov. 27, 2013) shows uplift centered on Uturuncu. Black and white circles are station locations. Small black circles are catalog earthquake locations.

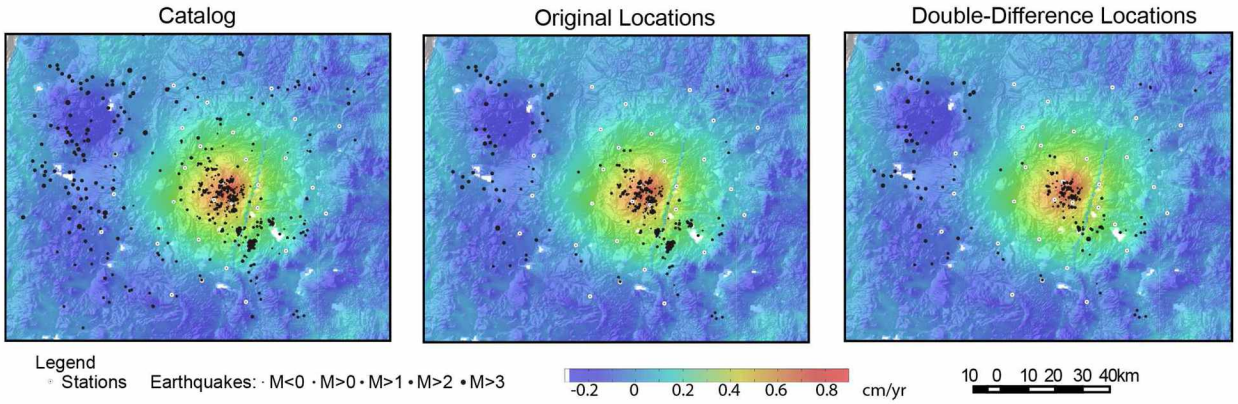

Figure 2.2 Earthquake Locations.
(left) Locations of all 592 earthquakes in the catalog. (center) Original locations of the 413 earthquakes that are used during relocation. This is a subset of the total catalog. (right) Double-difference locations of the 410 earthquakes that were relocated.

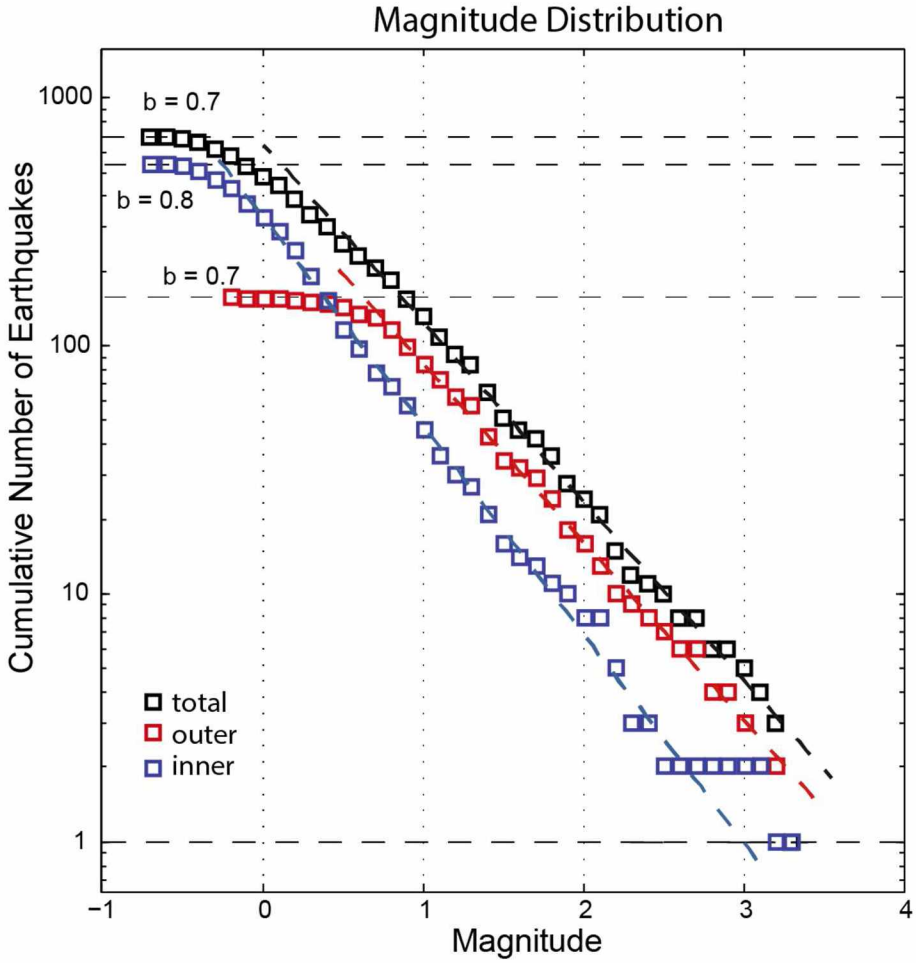

Figure 2.3 Magnitude Distribution of the Earthquake Catalog.
The magnitude distribution and b-value of the catalog vary with location. Earthquakes within the array (blue) have a higher b-value and lower magnitude of completeness than those outside of the array (red).

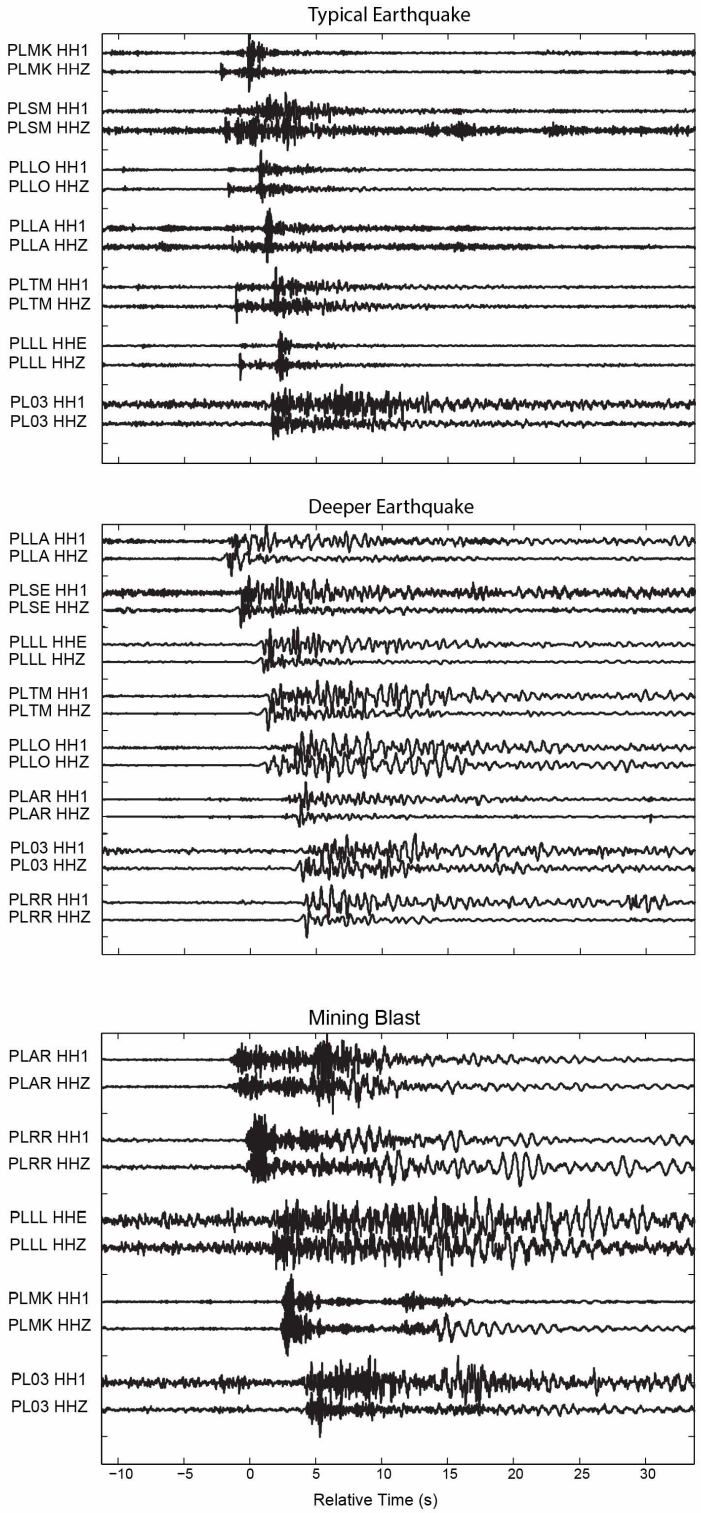

Figure 2.4 Waveforms of the three types of observed earthquakes.
(a) The majority of earthquakes recorded around Uturuncu are typical VT events with clear and distinct P and S arrivals. (b) Earthquakes that appear to have the high frequency and shear motion attenuated. (c) Mining blasts.

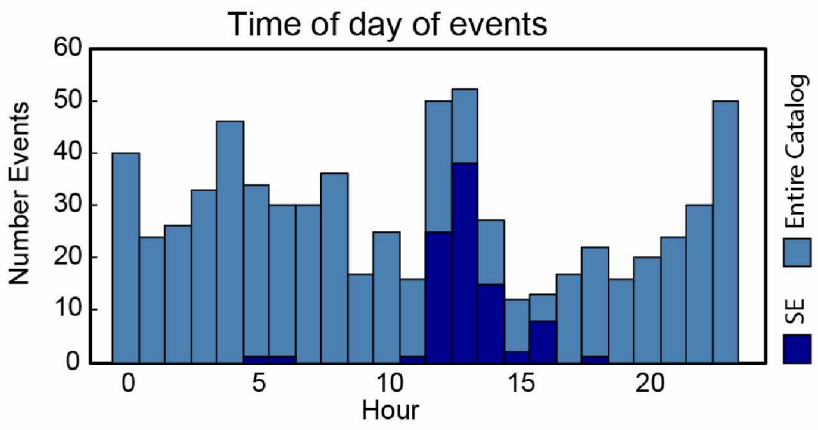

Figure 2.5 Histogram of the Time of Day of Earthquakes in the Catalog.
Light blue bars show the hours of the entire catalog –including the events in dark blue. Dark blue are the events to the southeast of the array (SE, the region south of 22.3 S and east of 66.9 W) that have the typical "mining blast" appearance to their spectral content. The limited time range of these events suggests that they are in fact mining events. Therefore, they are not included in our relocations.

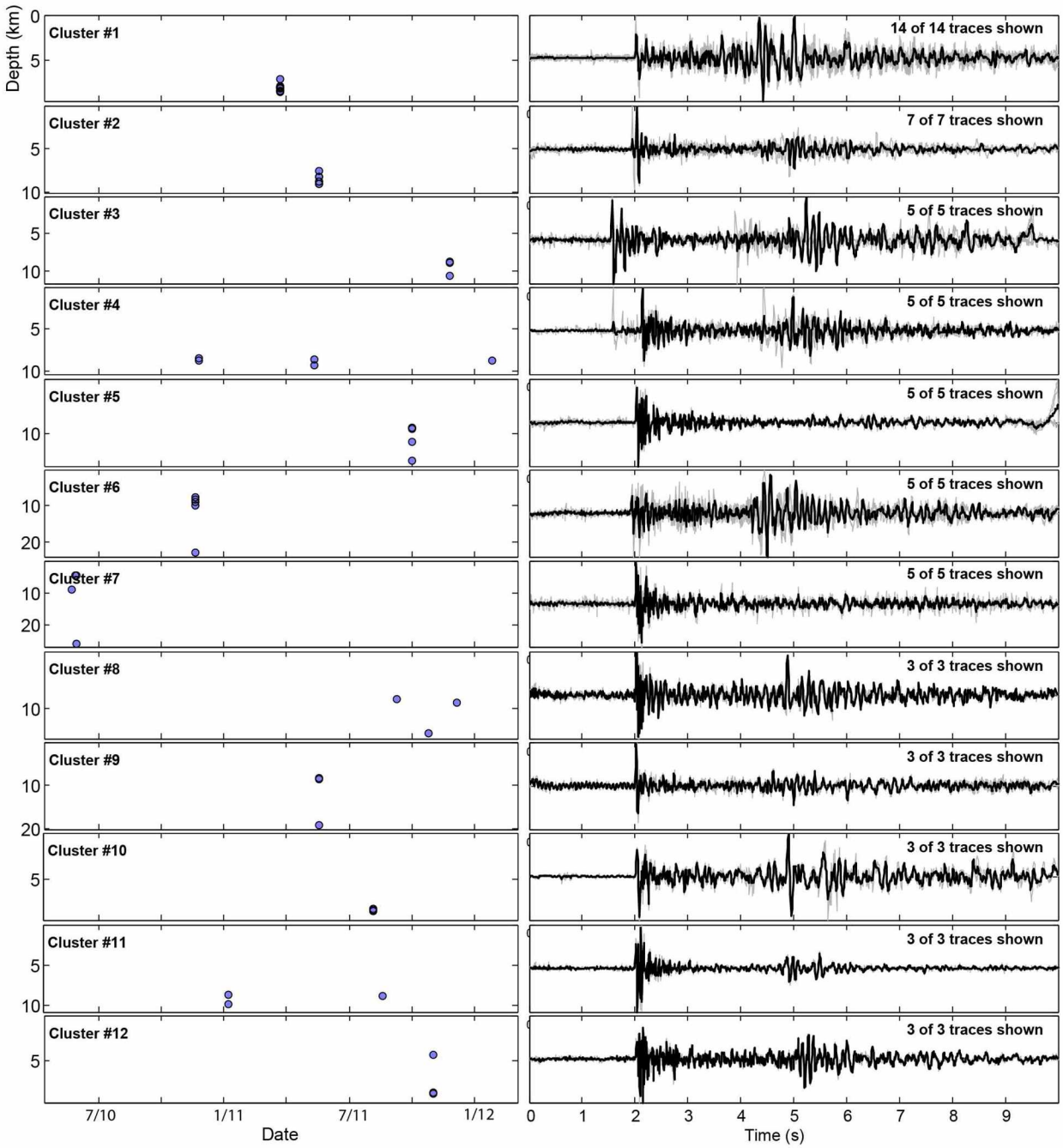

Figure 2.6 Waveforms and Depths of the 12 Largest Families.
(left) Depth vs. Time plot that includes the earthquakes in each of the 12 largest families. (right) Light grey are the individual waveforms for each earthquake in the family. Black is the stacked waveform for the family. All waveforms are high pass filtered above 1.0 Hz.

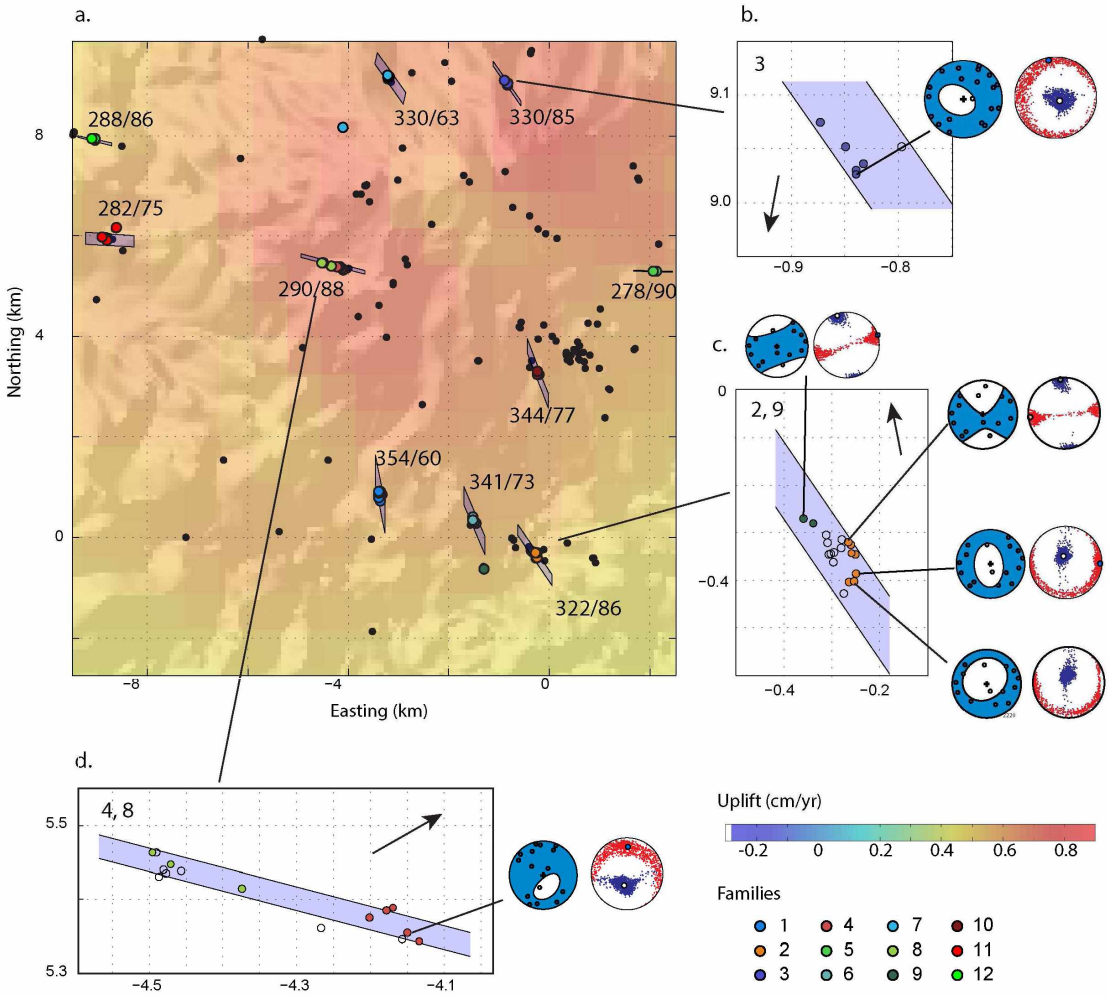

Figure 2.7 Focal Mechanisms and Planes Fit to the Largest Families.
(a) Map view of the 12 families with the most earthquakes, colored by family. Blue polygons are best-fit planes to each of the families, with very nearby families combined. Numbers by each family indicates the strike of the plane. Northing and eastings are relative to the center of double-difference cluster used during relocation. (b) - (d) Families for which we have focal mechanisms. Light blue shaded regions indicate best fit plane; arrow indicates direction to the summit of Uturuncu. For the events that have focal mechanisms calculated, both a randomly selected focal mechanism and the P (blue) & T (red) axes of 1000 possible solutions are plotted. Focal mechanisms are from Alvizuri and Tape (2014).

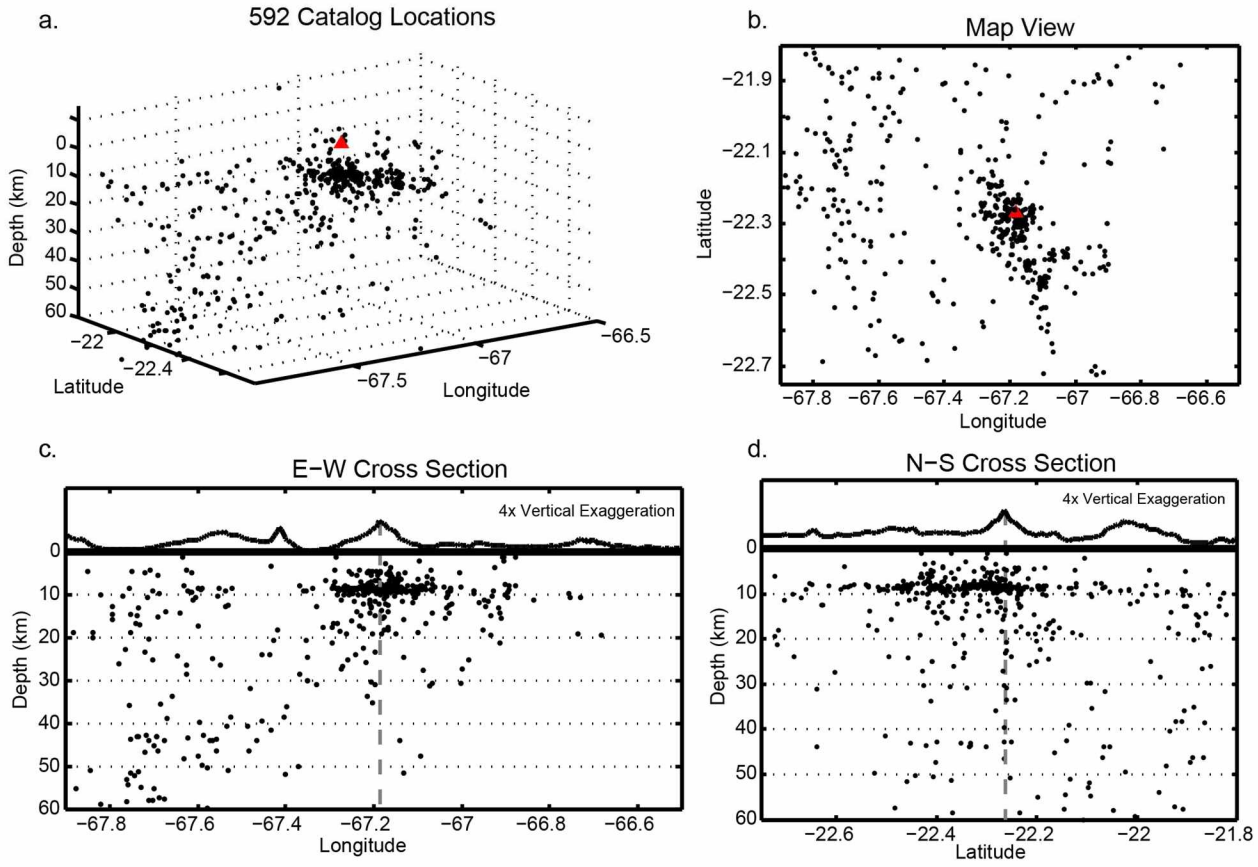

Figure 2.8 Cross-Sectional Views of Catalog Locations.
The original catalog locations, with mining blasts excluded. The red triangles in the top panes mark the location of the summit of Uturuncu. The bottom panes show a 4x vertically exaggerated topography, with the summit of Uturuncu marked with the grey dashed line; no vertical exaggeration below the surface. Depths are relative to the surface.

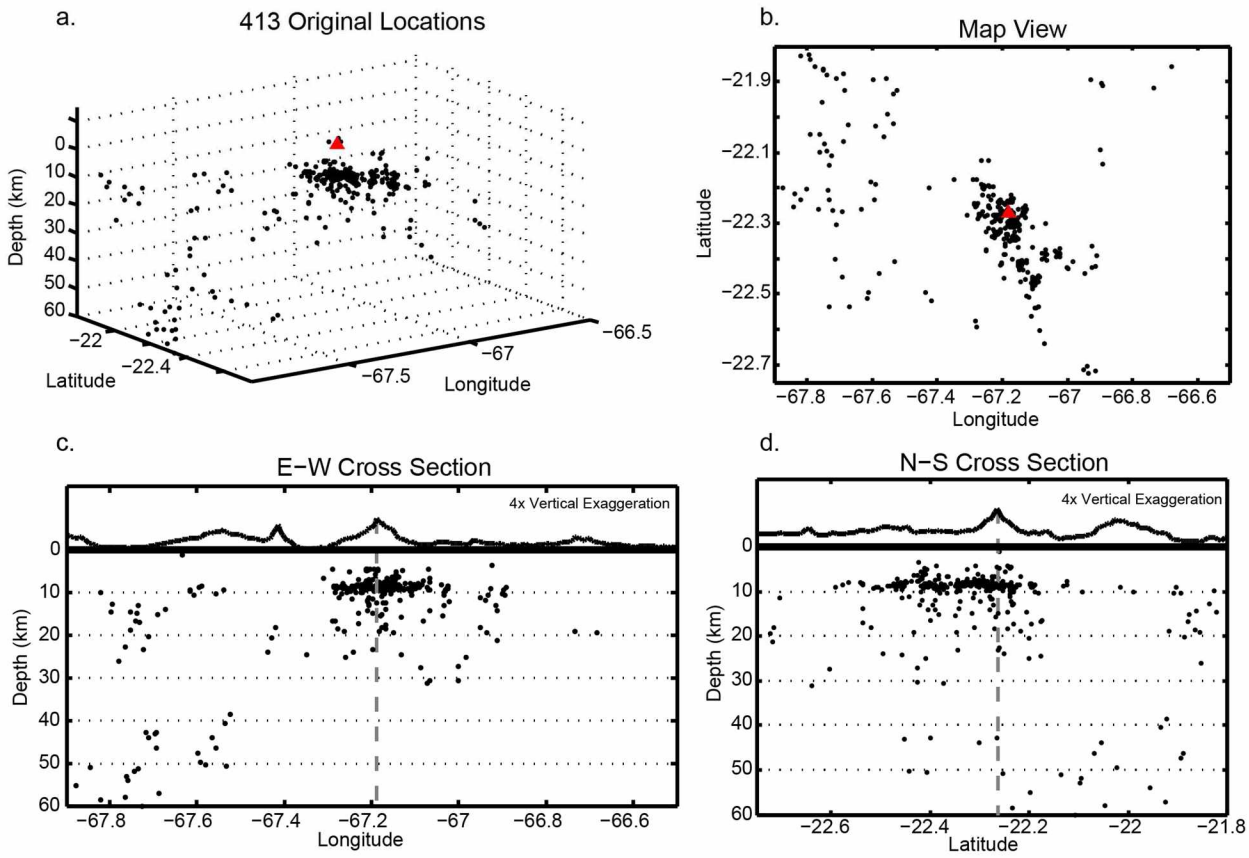

Figure 2.9 Cross-Sectional Views of Original Locations.
The earthquakes that are used during relocation. The locations are the same as in Figure 2.9, but only the subset used during relocation are shown. The red triangles in the top panes mark the location of the summit of Uturuncu. The bottom panes show a 4x vertically exaggerated topography, with the summit of Uturuncu marked with the grey dashed line; no vertical exaggeration below the surface. Depths are relative to the surface.

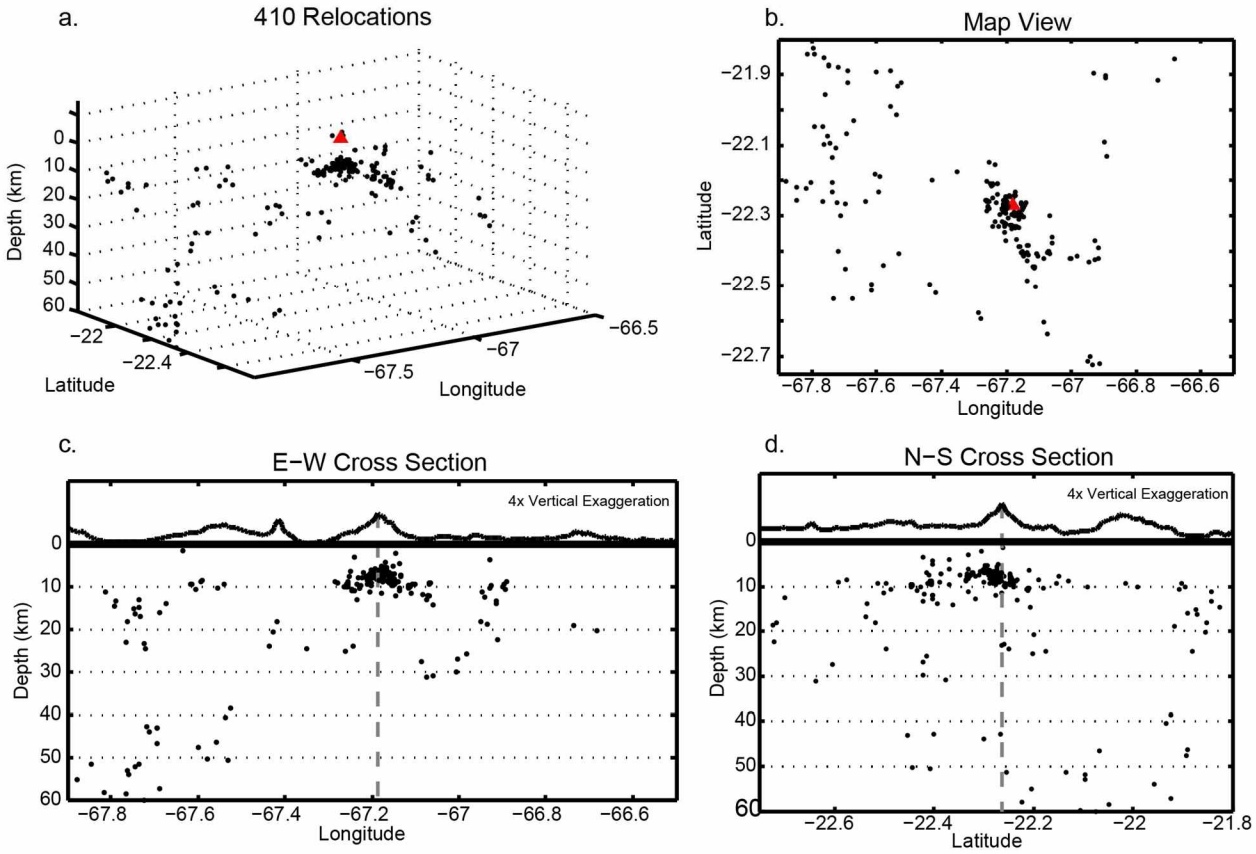

Figure 2.10 Cross-Sectional Views of the Double-Difference Locations.
The double-difference locations. The red triangles in the top panes mark the location of the summit of Uturuncu. The bottom panes show a 4x vertically exaggerated topography, with the summit of Uturuncu marked with the grey dashed line; no vertical exaggeration below the surface. Depths are relative to the surface.

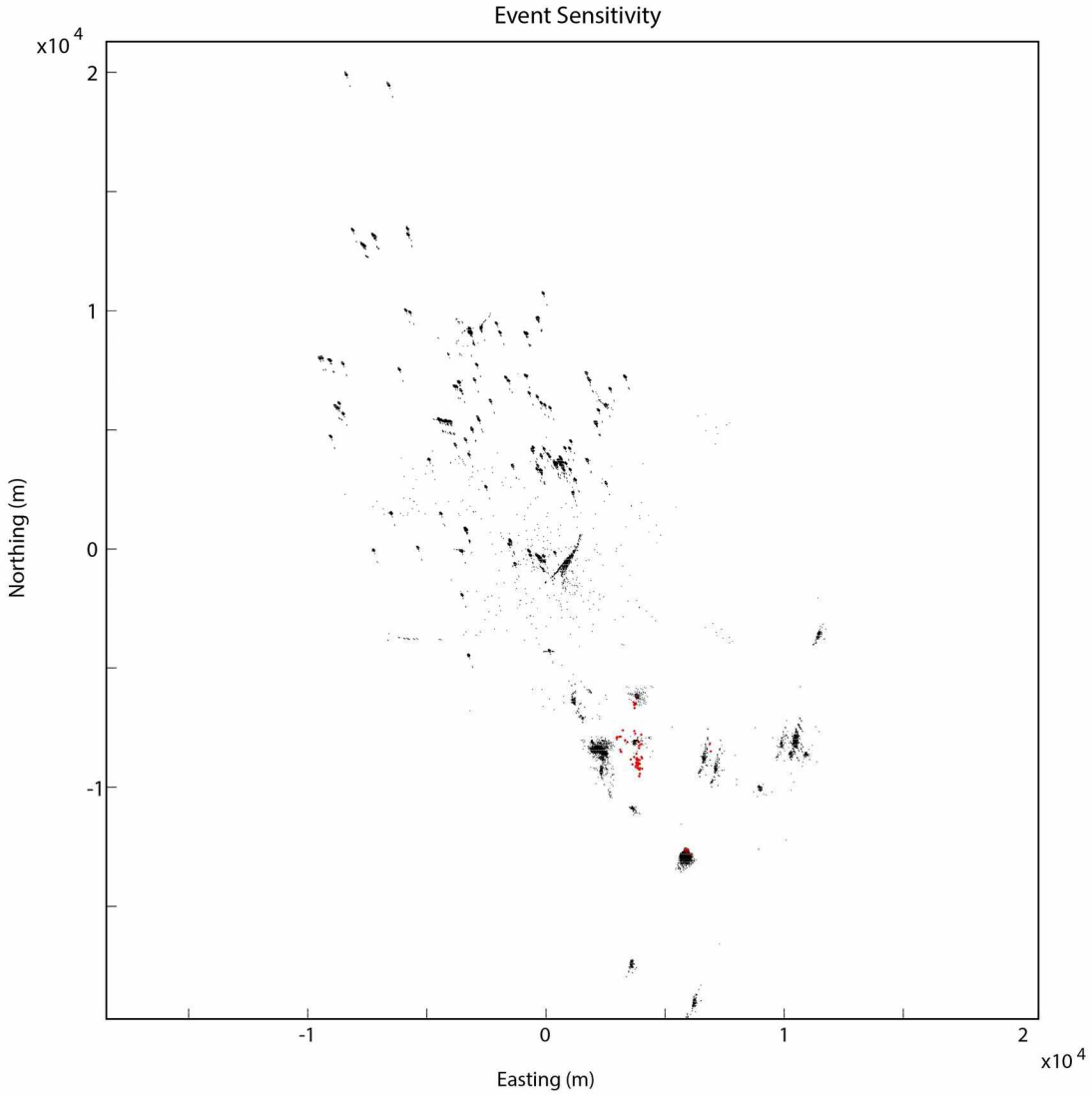

Figure 2.11 Event Sensitivity Test.
All earthquake locations are plotted for all 592 event sensitivity runs. Each cloud is "one" earthquake. The red dots are the locations of one randomly selected earthquake.

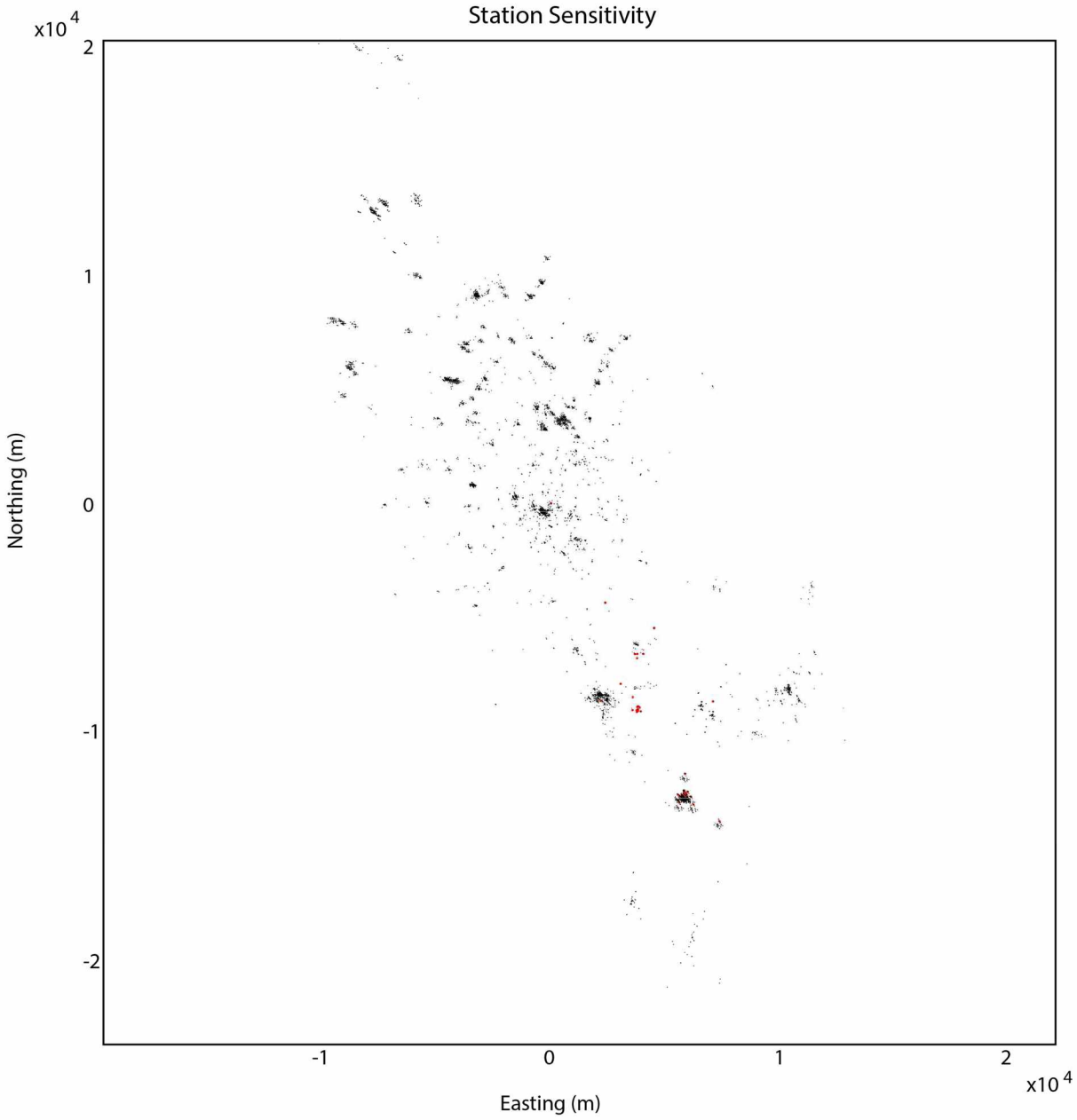

Figure 2.12 Station Sensitivity Test.
All earthquake locations are plotted for all station sensitivity runs. Each cloud is "one" earthquake. The red dots are the locations of one randomly selected earthquake.

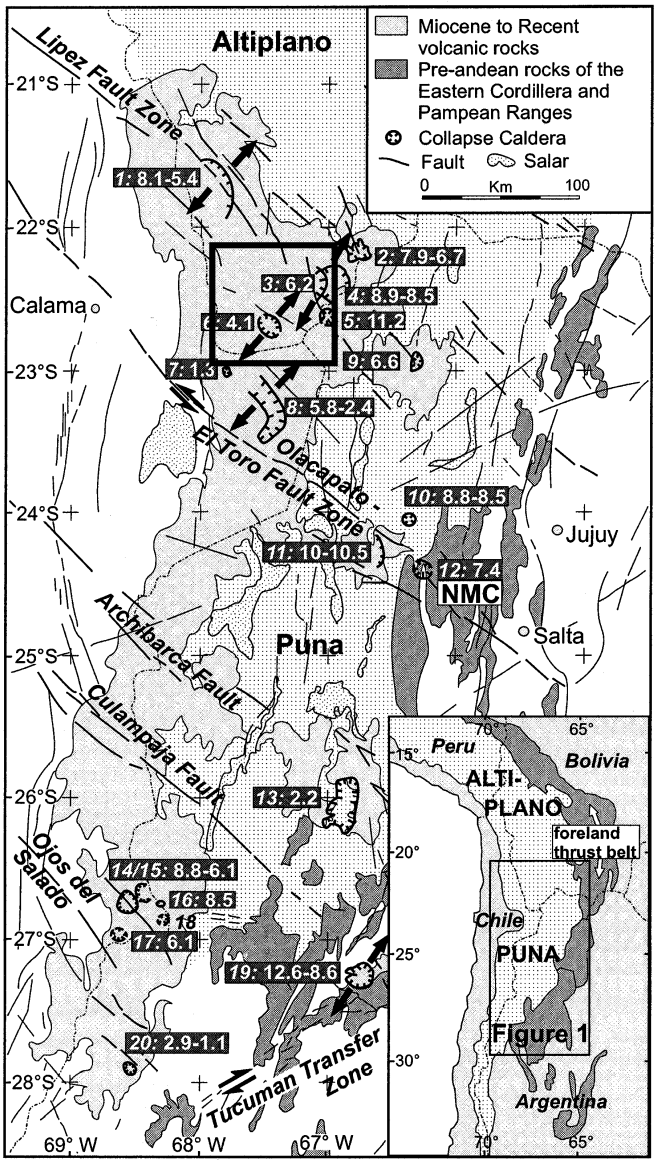

Figure 2.13 Fault Map of Southern Bolivia and Northern Chile.
From Riller (2001), the fault map shows a series of NW-striking strike-slip faults. At the northern end is the Lipez-Coranzuli fault zone, which cuts past Uturuncu volcano. The black box marks the region with Uturuncu.

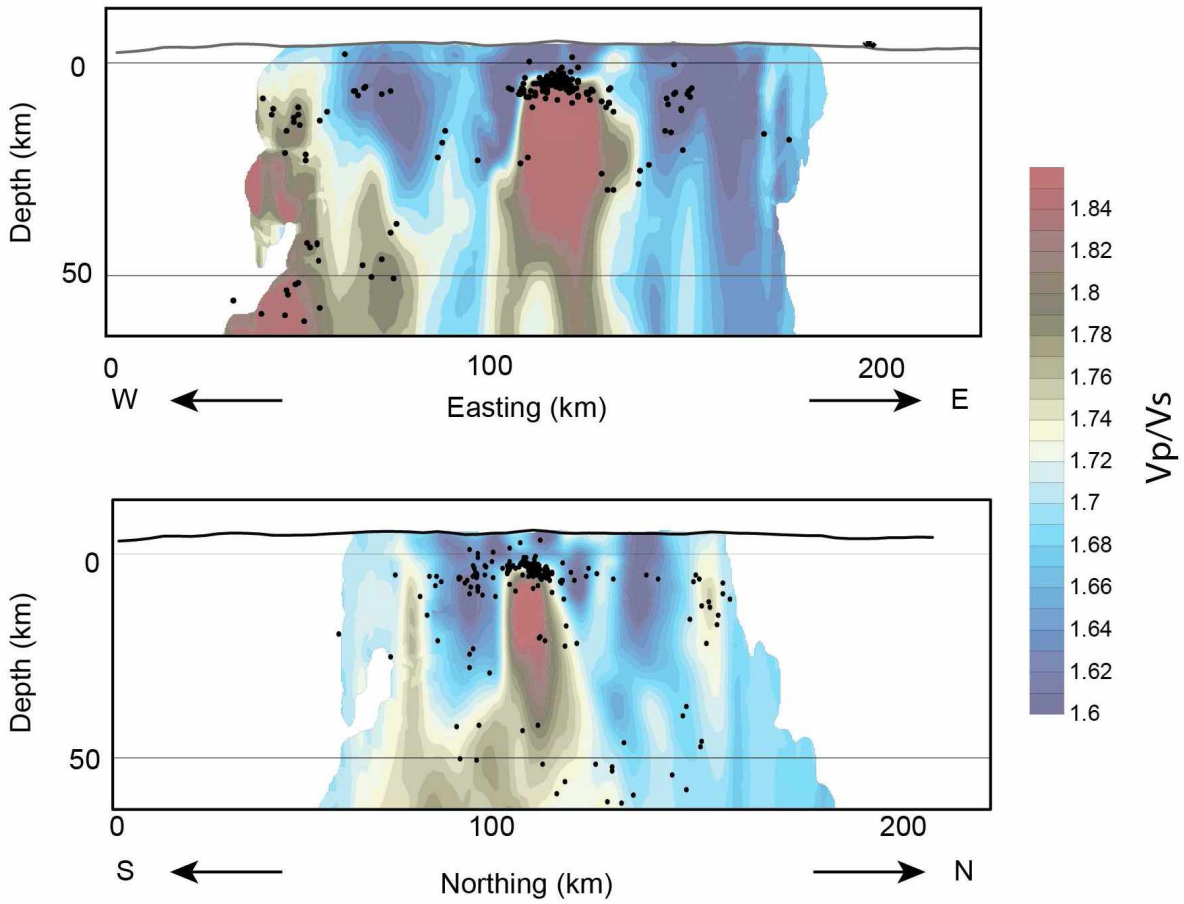

Figure 2.14 Seismicity with Vp/Vs Tomography.
Relocated seismicity plotted with Vp/Vs ratios from West *et al.* (2013). High Vp/Vs ratios are interpreted as low shear velocities associated with increased melt. While the vertical extent of the velocity anomaly is poorly constrained, the excellent horizontal alignment of the seismicity with the high Vp/Vs zone further supports the suggestion that the seismicity is located at the top of the diapir. Note that all relocated earthquakes are included in the cross sections, not just those near the low velocity zone. Depths are relative to sea level.

Table 2.1 Velocity Models.
(top) Velocity model used during double-difference relocations. (bottom) Model used during original location.

	Top of Layer (km below sea level)	Vp
DD Velocity model	-4	4.1
	15	6.2
	35	7
	70	7.7
	100	8.0
	150	8.1
	400	8.5
utu03	-3	4.2
	5	5.7
	40	7.5
	70	7.6
	110	7.8
	200	8

Table 2.2 Sensitivity Test Results.
Standard deviation, in meters, of earthquake locations during the Jackknife sensitivity tests for Event and Station.

	X (m)	Y (m)	Z (m)
Event	112.6	144.5	94.6
Station	478.6	800.9	398.9

Chapter 3 Double-Difference Relocation of Interior Alaska Seismicity[1]

3.1 Introduction

On Sunday, August 31 at 3:06 UTC, an M_L 5.1 earthquake occurred near Minto, Alaska. Analysts at the Alaska Earthquake Center (AEC) located it at 70 km to the northwest of Fairbanks and at a depth of 16 km, placing it near the northern extent of the Minto Flats Seismic Zone (MFSZ). Within two months of the initial event, we recorded two more earthquakes of M_l 5, as well as over 1700 smaller aftershocks.

Initial interpretations of fault orientation and sense of slip were based on the focal mechanism of the mainshock. The majority of earthquakes within the MFSZ fall along two NE-striking strands of seismicity, which align with one of the focal planes of the August 31 earthquake. This made it a natural candidate for the assumed fault plane, at least initially. As the aftershocks continued, however, this assumption was questioned as they mapped out a roughly NW-trending area. Earthquake locations fell along an elongate, diffuse cloud roughly aligned with location errors. For this reason, we conducted further analysis of aftershock data that suggests that these large events did indeed take place on a previously unknown fault that runs perpendicular to the MFSZ.

The results from this earthquake sequence prompted the re-examination of two other large events in the region in order to investigate whether they also occurred on conjugate faults or whether they align with the MFSZ. The goals of this study are to 1) investigate the fault planes associated with the earthquakes since there are no surface ruptures or otherwise mapped faults in the vicinity, and 2) improve our understanding of the structure of the northern end of the MFSZ.

Additionally, we performed relocations on the entire catalog of Interior earthquakes, M>0.8. This provided a framework to analyze the Minto-area seismicity as well as improved our understanding of tectonics of the Interior as a whole.

3.2 Setting

Subduction of the Pacific plate under the North American plate in southern Alaska generates stresses that are the source of a large portion of the seismicity in Alaska, both directly

[1] Hutchinson, L.K., M.E. West, and C. Tape, 2015. Double-Difference Relocation of Interior Alaska Seismicity. Prepared for submission in *Seismological Research Letters*.

in the subduction zone and indirectly elsewhere (Figure 3.1). At the eastern edge of the subduction zone, there is evidence for the subduction of over-thickened crustal material, termed the Yakutat block. It is believed that this thick, mafic material produces flat-slab subduction in the region (Fuis *et al.*, 2008), pushing the related volcanic arc inland, generating a high rate of seismicity in the region, and increasing coupling with the North American plate (Jadamec *et al.*, 2013).

Materials escape westward to the south of the Denali Fault through counter-clockwise motion of the Wrangell Block (Lahr and Plafker, 1980). Jadamec *et al.* (2013) found that motion along the Wrangell block can be modeled as the result of coupling with the Yakutat flat-slab subduction. The northern edge of this block is the Denali Fault, an arcuate dextral fault that cuts through the Alaska Range. Motions of up to 400 km have been documented along the eastern portion of the fault, though such evidence is lacking to the west.

Alaska's Interior is a broad region of active deformation bound by the Denali Fault to the south and the Tintina/Kaltag fault systems to the north. Despite a lack of mapped faults with Holocene motion in the region, the Alaska Earthquake Center has recorded over 23,000 earthquakes in the area since 1975 (Figure 3.2). The most striking feature of the Interior seismicity is the NNE-SSW trend to the handful of seismic zones that have been identified, including the Minto Flats Seismic Zone (MFSZ), the Fairbanks Seismic Zone (FSZ), and the Salcha Seismic Zone (SSZ). These zones all produce predominantly sinistral strike-slip earthquakes and have produced a series of larger events in the past (e.g. Ms 7.3 in 1904, Ms 7.3 in 1937, Ms 7.2 in 1947; Page *et al,*. 1995). Studies show that the total strain rate across the seismic zones is small, at a maximum of 0.2 mm/yr across any given seismic zone (Fletcher, 2002). To the east, where seismicity is quieter, there is a series of mapped lineaments and faults that strike NE-SW (Plafker *et al.*, 1994). There are two competing models for the source of deformation in the Interior: the clockwise rotation of the Bering Block, and block rotation within the Interior.

The proposed Bering block encompasses the majority of the Bering Sea. This model stems from seismic patterns in western Alaska and eastern Russia, which – it has been suggested – is best explained by the clockwise rotation of the Bering block (Lahr and Plafker, 1980; Mackey *et al.*, 1997). GPS data also support the idea of a rigid Bering block (Cross and Freymueller, 2008).

The eastern-most extent of this block is poorly defined and has been suggested to lie as far east as the western edge of the Wrangell block (Lahr and Plafker, 1980) in the south and along the Kaltag fault in the north. Clockwise rotation could explain both the decreased motion along the western portion of the Denali fault, as well as the left-lateral faulting in the Interior (Cross and Freymueller, 2008). But, the right-lateral motion of the Kaltag Fault does not match the predicted motion of the Bering block. This suggests that the rotation of the Bering block may not be the driving mechanism for seismicity in the Interior, or at least that the model as is needs to be adjusted.

Alternatively, it has been suggested that the seismic zones are produced by a series of rotating blocks driven by compression and shearing of the Interior. Based on seismic patterns and focal mechanisms, Estabrook *et al.* (1988) concluded that the Interior is a large-scale, low-strain shear zone. Page *et al.* (1995) proposed that seismicity is due to block rotation, caused by shearing, bound to the north and south by the two major strike-slip faults. In this model, block rotation accommodates roughly north-south shortening caused by convergence of the Pacific and North American plates. Indentation along a curved plane should produce variations in the stress pattern from east to west. There are mapped (albeit seismically quiet) faults to the east strike more northeast than those further west; this longitudinal variation of the maximum horizontal stresses is consistent with the expected pattern due to compression of the North American-Pacific plate convergence (Estabrook and Jacob, 1991).

3.3 The Minto Flats Seismic Zone

Of the seismic zones listed above, the longest and most prominent is the Minto Flats Seismic Zone (MFSZ). From the Denali Fault in the south, the MFSZ reaches 200 km to the northeast where it runs approximately 45 km to the west of Fairbanks (Figure 3.2). There is no surface expression of the MFSZ, as such, we must rely on seismic data to map out the faults in the region.

The northern part of the MFSZ consists of two strands of sub-parallel, seismically active lineaments that appear to have a classic pull-apart basin between them (Figure 3.2). While the mechanism for basin formation is under debate, the 8 km deep basin (Doyon Limited, 2012) is marked by high levels of seismicity throughout the basement. This pattern indicates that the

basement may be highly fractured and that deformation is distributed amongst the network of faults. Doyon Limited (2012) studies show a pattern of offset basement blocks, which would be consistent with a network of faults throughout the basin.

The MFSZ is the source of over 35% of the total seismicity of the Interior. The Interior, for the sake of this study, is the rectangular area bound by (145W, 64N) and (151W, 65.7N). Note that this does not include the Kantishna cluster, which is another prominent source of seismicity. Our catalog spans the time period from 1975 through October 2014. Of the 9365 earthquakes larger than the magnitude of completeness for the Interior (Mc 1.2), over 3,500 occurred in the MFSZ. Of the total seismic energy released in the Interior, the MFSZ has generated 90% in the timeframe of this dataset. This value is dominated by the 1995 M_l 6.2 but demonstrates how active the MFSZ is relative to the rest of the Interior in the past 40 years. The five largest events of the Interior from this timeframe occurred in the MFSZ, all of which are also a part of the three sequences of this study.

Given the length of the seismic zone and the fact that it has produced a number of larger earthquakes, this region is a dominant earthquake hazard in the Fairbanks area. It is important to have a good grasp on the extent of the faults and style of faulting in the area. Despite the importance of the MFSZ to seismic hazards in the Fairbanks region, the confluence of modest station coverage, a lack of geologic expression, and somewhat deep earthquake locations all conspire to make these sequences challenging to investigate.

3.4 The Three Minto-Area Sequences

This study focuses on three earthquakes and their aftershock sequences. They have been chosen for a number of reasons, but one of the primary factors is that this method requires that there is a dense concentration of earthquakes, sufficient to map the fault plane that they occurred on. These events, at M_l 5.1 (2014), M_w 6.2 (1995), and M_l 5.0 (1990), are large enough to provide this through their aftershock sequences. Additionally, these events are located spatially nearby each other, which means that they a) should be expressions of the same stress regime, b) can be used to help us map out the structure of the northern extent of the seismic zone, and c) can all use the same relocation parameters and be run together as a single cluster to improve the spatial relationship between the three sequences.

2014 Sequence

While it was recorded as a single event, the event on August 31th, 2014 at 3:06 UTC was actually two earthquakes separated by 1.4 s. Unfortunately, this was too close in time to locate the two earthquakes individually, and as such they are treated as a single event both in the catalog and here.

The M_l 5.1 was widely felt and prompted 331 Did You Feel It (DYFI) reports from Minto to Delta Junction (229 miles away), with a maximum intensity of VI on the Modified Mercalli Intensity Scale (MMI) recorded in Nenana and a MMI of IV in Fairbanks. The MMI provides a measure for the effect of the earthquake, including how much ground shaking and destruction it caused. An MMI of IV-VI indicates light to strong shaking with slight damage.

Over 1700 earthquakes were recorded during the two months after the mainshock, with a magnitude of completeness of M_l 0.3 (Figure 3.3). Aftershock magnitudes range from M_l -0.02 to M_l 5.0. The sequence, as a whole, does not fit Omori's predicted aftershock decay rate. While the number of earthquakes does decay with time, two M5 earthquakes occurred a month and a half after the main August earthquake. In order to compare the aftershock rates from this earthquake sequence to those from the 1990s, we looked at the normalized cumulative number of earthquakes with time. This gives us a sense of how quickly the sequence died out, or how productive the aftershocks were (Figure 3.4; Figure 3.5). Because the two M5 earthquakes generated their own aftershock sequences, we compared only the timeframe from the mainshock until the first M5 aftershock.

The first of the two M_l 5.0 earthquakes occurred at 00:36 UTC on Tuesday October 21, 2014. Analysts located it at nearly the same place as the August 31 event and calculated a similar focal mechanism, suggesting that it occurred on the same fault.

This event was followed by another M_l 5.0 two days later on October 23 at 16:30 UTC. 136 DYFI reports were submitted, which again indicated that the region around Fairbanks experienced the greatest ground shaking with an MMI of IV. Two DYFI reports were submitted

from Minto, describing light to moderate shaking there as well. The weaker shaking reported in Minto is likely the result of the small sample size in Minto, though.

In general, station coverage can strongly affect the number, location, and magnitude of completeness of the recorded earthquakes. Station coverage in Alaska, and the Interior in particular, has improved throughout the past few decades, and as such this earthquake sequence was better recorded than the two from the 1990s (Figure 3.6). This sequence is well recorded to the south, where we use data from 68 stations. To the north of the Fairbanks area, coverage is sparser – there we are able to use data from 10 stations. Over 1,000 earthquakes have P arrivals picked at 10 or more stations, meaning that this sequence was well recorded.

The entirety of this aftershock sequence occurs to the northwest of the MFSZ by approximately 15-20 km, in a relatively diffuse NW-SE cloud of seismicity. Errors assigned for the catalog locations align roughly with the direction of the cloud, with maximum horizontal errors averaging 1.4 km (one standard deviation), striking an average of 279° (Figure 3.7).

1990 Sequence

On January 07, 1990 at 11:01 UTC, an M_l 5.0 occurred in the region just south of the 2014 earthquakes. Approximately 50 aftershocks of M_l 1.0 – M_l 3.0 were recorded for this sequence. Catalog locations show that the events spanned a distance of approximately 20 km and ranged in depth between the surface and 24 km. Maximum horizontal errors average 3 km, striking to the northeast.

In 1990, the seismic network was much less dense than it is now, and only 27 stations were able to record the events. The vast majority of the picks occurred on only 7 stations. This led to a much higher magnitude of completeness and a much scarcer record of the aftershock sequence (Figure 3.3). Station coverage is isolated to southwest of the sequence, with the closest station at approximately 50 km to the west. As such, the rupture plane is more difficult to determine than for the 2014 events.

1995 Sequence

The M_w 6.0 earthquake that occurred on October 6, 1995 was felt strongly in Fairbanks and caused minor property damage (Ratchkovski and Hansen, 2002). Approximately 400

aftershocks were recorded in the two months after the mainshock, ranging from M_l -0.4 to M_l 4.5. Due in part to the larger size of the mainshock, and in part to the improved network since the 1990 earthquake, events were recorded at 127 stations, with 10 stations recording nearly every earthquake.

Unlike the other two sequences, these events occurred near the northern end of the MFSZ, essentially in line with the strike of the seismic zone. The average maximum horizontal errors are 3.6 km, striking an average of 154 degrees.

This event was examined by Ratchkovski and Hansen (2002) and relocated using the joint hypocenter determination (JHD) method. Here, we reprocess the aftershock locations using double-difference in order to a) include waveform cross-correlation data, and b) ensure that the results from this sequence can be directly compared to the other two by using the same relocation methods and parameters.

3.5 Double-Difference Relocations

To improve constraints on the orientation, extent, and structure of the faults that produced the three sequences, and for the Interior as a whole, we performed double-difference relocations on the analyst-reviewed earthquakes using the program hypoDD (Waldhauser, 2012). Double-difference relocation is a method that utilizes travel time differences for paired events to produce improved relative locations. The fundamental assumption is that energy from both earthquakes travel along essentially the same path as it reaches the seismometer. Given that assumption, any difference in travel time for the two earthquakes is a result of slight difference in location rather than a difference in path velocities. By pairing nearby events in this way, many station- and path-related errors are minimized (Waldhauser and Ellsworth, 2000).

While using catalog travel times improves the relative locations, we can do better by using cross-correlations to correct for inconsistent picking. We use both P and S travel times and perform cross-correlations over a window of 1.0 s. We use a short window to increase the number of pairs that meet the minimum correlation value threshold and therefore increase the amount correlation data used during relocation. Since the goal is to align the initial arrivals, we are not concerned with generating families of similar events or, therefore, correlating large

portions of the waveform. For this study, pairs must meet a minimum correlation value of 0.7 in order to calculate cross-correlation differential times to be used for relocation.

We used a modified version of the velocity model that the Alaska Earthquake Center uses to locate events in central and northern Alaska. We decreased the velocity of the uppermost layer to 4.9 km/s (rather than the original 5.9 km/s). This was done in part because the events take place near the northern extent of the Nenana Basin, which is known to be a deep basin filled with sediment and believed to be highly fractured. Because double-difference relocation uses the travel time difference to calculate the spatial difference between two earthquakes, it is important that the model velocity reflect the true velocity at the location of the earthquakes. The second reason we decreased the velocity is because of the number of airquakes, events that are mislocated to above the ground surface, being located during the double-difference process with the original velocity model. Velocities that are too fast will both decrease the depth of the earthquakes and increase the distance between them, producing airquakes. The value 4.9 km/s was chosen by systematically varying the velocity and determining which value decreased the number of airquakes and reduced the RMS residuals for both the catalog and cross-correlation data, while still maintaining a high number of earthquakes through the relocation process.

To quantify the dependence of the final locations on factors such as station distribution, event selection, and velocity model, we performed a number of sensitivity tests using the Jackknife method. Earthquakes were relocated repeatedly, each time eliminating a single event or station. Additionally, we relocated all earthquakes using all stations 40 times, varying the velocity of the top layer of our model in 0.1 km/s increments between 3.9 km/s and 7.8 km/s.

The results from those tests are used to calculate a variance estimate (and standard deviation) of the earthquake locations.

Interior Results

Relocations of the Interior seismicity were performed using the same parameters as for the three sequences. We relocated all earthquakes from 1975 to October 2014 of M>0.8. All quarry events were removed from the catalog prior to relocation.

The results show a sharpening of the seismicity into distinct fault lines, hereafter referred to as faults based on the seismic interpretation (Figure 3.2). The Salcha Seismic Zone consists of

one line of NNE-striking seismicity, perhaps with a hint of WNW-directed seismicity near the southern end. The Fairbanks Seismic Zone consists of three main NNE faults cut by two noticeable WNW faults. Near the very southern end of the seismic zone there is what appears to be a poorly-defined WNW pattern to the seismicity. On the border between the Fairbanks Seismic Zone and the Minto Flats Seismic Zone lies another thin fault line. It has a distinct bend to it at around halfway along the line, as well as a subtle bend near the northern end. Finally, the Minto Flats Seismic Zone consists of the two main faults in addition to a well-defined line of seismicity to the west of the faults. As mentioned previously, the three sequences produce a series of WNW striking seismicity near the northern end of the seismic zone.

2014 results

To maintain consistency between this sequence and those of the 1990s, we relocated only the 230 earthquakes that are greater than M_l 1.5. This also allowed us to use only those events that were more widely recorded and had better signal-to-noise ratios, improving both the initial picks and the cross-correlations. All of these larger earthquakes are well enough connected – i.e., share greater than 8 observations with at least 8 other earthquakes - to be relocated.

After relocation, earthquake locations show a WNW-striking, steeply dipping fault plane. This plane is approximately 6 km long and 3-4 km wide, at 9 to 13 km depth. It strikes approximately 300° and dips 75° to the NNE (Figure 3.8), making it roughly 90 degrees off of the NW strand of the MFSZ.

Sensitivity tests show that locations are relatively stable (Figure 3.9; Figure 3.10). Locations in the event test shift by a standard deviation (σ) of around 50 m in the horizontals and up to approximately 225 m vertically (Table 3.2). Locations have a greater dependence on stations, with σ values ranging from 130-390 m.

1990 results

For this sequence, we decided to use all events rather than limiting ourselves to only those that are M1.5 or greater. This is because the sequence is already fairly small, and eliminating the smallest events reduces the dataset too far. Relocations are not greatly changed from the catalog locations, likely due to the poor station coverage. But there is some greater constraint on event

depths without a change in plane strike, indicating that the events really do fall on a fault that strikes northwest.

This plane strikes approximately 330° and dips nearly vertically. It appears that the earthquakes fall on a part of the fault that is 17 km long and 5-15 km wide (Figure 3.10). A rupture area of that size is large for a M5 earthquake, which suggests that perhaps the events included in the study outline more of the fault than was ruptured during the mainshock. This would not be surprising given there have been other earthquakes that have occurred in line with the plane mapped out during this event (Figure 3.2). Indeed, this earthquake appears to occur on a fault that intersects the eastern strand of the MFSZ.

Much like the 2014 sequence, sensitivity tests show that stations have a greater impact on location than events (Figure 3.9; Figure 3.10), with horizontal σ ranging from less than 100 m (event) to approximately 250 m (station) (Table 3.2). Depth uncertainties range from σ of 225 m for event tests to just under 800 m for station tests.

1995 results

297 earthquakes of M_l 1.5 and larger were used during the relocation process and the results from this year are much more ambiguous than those from the other two years. It does not produce one nice fault plane, though the events do seem to cluster more densely on one plane (Figure 3.12). The definition of this plane depends greatly on the velocity model used and the vertical extent largely disappears with decreased velocities (such as the 4.9 km/s used in this study). In addition to the denser cluster of events in the northeast-southwest direction, there is also a cloud of events in the northwest-southeast direction. Because this result is produced using the same parameters and as a part of the same cluster as the 2014 events, which fall onto a nice fault plane, and because station coverage is not drastically different between those two years, we are inclined to believe that the diffuse northwest-southeast trend is also real.

While we must be careful in interpreting any planar fits to this relatively complicated aftershock sequence, for the sake of discussion we provide fits to both the NW-SE and the NE-SW trends to the seismicity. First, fitting the entire aftershock sequence produces a plane that strikes approximately 320° and dips 55°. When we fit a plane to just those earthquakes that

cluster in the densest part of the sequence, we get a nearly vertical plane that strikes approximately 10° (Figure 3.12).

Event sensitivity tests (Figure 3.9) show horizontal σ values of under 100 m and a vertical σ of just over 200 m (Table 3.2). Station tests have σ values that range from 300- 600 m (Figure 3.10).

3.6 Discussion

All three earthquake sequences investigated in this study have at least a component of WNW-striking orientation to the aftershocks. Both the 2014 and the 1990 earthquakes and their aftershocks appear to have occurred on WNW-striking faults. This is in contrast to the 1995 earthquake which likely ruptured along a NNE-striking plane. The majority of the aftershocks cluster along the NNE plane, though there are a considerable number of aftershocks that map out a relatively diffuse, WNW-ESE region surrounding the mainshock.

Relocations of the entire Interior show sharpening of the seismic zones into a series of more coherent faults. These are roughly parallel with each other, with an average spacing of ~15 km. In addition, we see a set of cross-faults that have spacing of around 50 km.

Cross-faulting within the Interior has not been investigated extensively in the literature. But, as the three largest events that have occurred in the northern end of the MFSZ in the last 25 years demonstrate rupture along WNW faults, and Interior relocations support the possibility of cross-faults throughout the Interior, it is important to consider their role in the tectonics of the region. Here we investigate two possible mechanisms for the formation of these faults: block rotation and conjugate faulting.

Block Rotation

One of the most prevalent theories is that Interior seismicity is generated by block rotation due to compression and shearing of the Interior. In the block rotation model, it is expected that seismicity will occur on all edges of the blocks, not just the east and west borders. The seismic zones in the Interior do not appear to fill the entire distance between the Denali and the Tintina faults, so there should be some expression of the northern and southern edges. Perhaps these cross-faults represent the northern end of a rotating block (Figure 3.13). This is an especially

tempting explanation, as the NW faults associated with the 1995 and 2014 earthquakes are orthogonal to the MFSZ. But, the expected sense of slip of a clockwise rotating block is left lateral, and the dextral motions of these faults are fundamentally incompatible with that of block rotation. Therefore, the cross-faults are not formed by block rotation.

Conjugate Faulting

Another explanation for the formation of these cross-faults is that they are a part of a conjugate fault system. In the classical Andersonian model of conjugate faulting, faults form at 30 degrees from the maximum stress direction, generating a system of faults at 60 degrees from each other (Anderson, 1951) (Figure 3.13). Of the Minto sequences, only the 1990 earthquake occurs on a fault approximately 60 degrees from the NNE strands of the MFSZ. The other two earthquakes are around 30 degrees from the expected angle. If there is indeed conjugate faulting at the northern end of the MFSZ, then either a) these WNW faults may have formed in a different stress regime and are simply reactivated by the current one, or b) faults do not necessarily form at 30 degrees off of the maximum compressive stress (e.g. Yin and Taylor, 2008). The third option is that the faults we find in this study are not conjugate faults. There are a number of examples of conjugate faulting systems with orthogonal faults, such as Central Honshu, Japan and the Salton trough, CA (Thatcher and Hill, 1991), so the fact that the 2014 and 1995 earthquake sequences are nearly perpendicular to the MFSZ does not in itself negate the possibility of conjugate faulting.

Stepping back, stresses are accommodated along longer NE-SW seismic zones as well as shorter NW-SE zones of seismicity throughout the Interior and particularly in the Fairbanks Seismic Zone (Figure 3.2; Figure 3.13). Here we observe the expected 60 degree angles, where the faults are 55-70 degrees from each other. In addition, focal mechanisms throughout the Interior show roughly the same pattern - NNE sinistral or WNW dextral motion (e.g. Ruppert *et al.,* 2008). While we cannot distinguish the actual plane from the auxiliary plane, the assumption that all earthquakes occur on the NNE plane is probably incorrect. This is especially true in complex regions where the cross-faults intersect. For those earthquakes that did occur on a

WNW plane, the dextral motion is in agreement with that predicted by conjugate faulting. As such, we conclude that there is in fact conjugate faulting occurring throughout the Interior.

The spacing of the WNW faults is very similar in the MFSZ and FSZ, suggesting that they are likely caused by the same process. While not impossible, it is unlikely that these highly similar faults (sense of slip, strike, and spacing) located within ~60 km of each other are unrelated. Indeed, although there is a lack of seismicity connecting the WNW faults of the FSZ and those of the MFSZ, the relative alignment of the faults in those two regions is intriguing. The connection between the faults of the FSZ and the MFSZ is speculative, but not unreasonable (Figure 3.13), especially given the observed bends in the fault that straddles the two seismic zones, where there appears to be dextral offset. These offsets could be due to motion along the WNW faults as they cross the NNE fault. If they are connected, there is the potential for much larger earthquakes on the conjugate faults than if they are discrete faults.

It bears pointing out that the fault associated with the 2014 earthquakes does not align with the conjugate faults of the FSZ, nor is it parallel with the fault of the 1990 earthquake. The difference in strike could be due to different stress fields within close proximity to each other, the re-triggering of an old fault that happens to be near optimal orientation, or the 2014 fault could be a part of some sort of interconnected or splay system that actually represents the same larger fault.

The 1995 sequence, with both the NE steeply-dipping plane and moderately-dipping NW plane, does not fit nicely into a model of slip along a single plane with aftershocks that map out the slip area. One possible explanation is that an event this large will apply stresses on nearby faults that subsequently ruptured as well. Doyon Ltd (2012) performed a depth-to-basement survey that has been interpreted as a series of NW and NE cross-faults offsetting crustal basement blocks. This interpretation could serve as a model of the northern end of the MFSZ. If the region surrounding the 1995 quake has the same fractured crust, the stress changes due to rupture on the main fault plane would doubtlessly apply new stresses to the surrounding faults that could cause rupture in a relative cloud around the mainshock. If the northern FSZ conjugate fault is indeed related to the seismicity of this region, then the cloud of seismicity would be on a fault (or faults) that had previously formed as a part of the conjugate fault system of the Interior.

3.7 References

Anderson, E. M. (1951), *The dynamics of faulting and dike formation with application to Britain.*, 2nd ed., Oliver and Boyd, Edinburgh.

Cross, R. S., and J. T. Freymueller (2008), Evidence for and implications of a Bering plate based on geodetic measurements from the Aleutians and western Alaska, *Journal of Geophysical Research*, *113*.

Doyon Limited (2012), Nenana Basin Depth Map, Available as an interactive website at `http://doyonoil.com/HiResImage/NenDepthMap-ForWeb`, last accessed 2015-04-12, depth data and countours from Gary Thompson

Estabrook, C. H., and K. H. Jacob (1991), Stress indicators in Alaska, in *Neotectonics of North America*, edited by B. D. Slemmons, Geological Society of America, Boulder, CO.

Estabrook, C. H., D. B. Stone, and J. N. Davies (1988), Seismotectonics of Northern Alaska, *Journal of Geophysical Research*, *93*(B10), 12026-12040.

Fletcher, H. J. (2002), Crustal deformation in Alaska measured using the Global Positioning System, 257.

Fuis, G. S., et al. (2008), Trans-Alaska Crustal Transect and continental evolution involving subduction underplating and synchronous foreland thrusting, *Geology*, *36*(3), 267-270.

Jadamec, M. A., M. I. Billen, and S. M. Roeske (2013), Three-dimensional numerical models of flat slab subduction and the Denali fault driving deformation in south-central Alaska, *Earth and Planetary Science Letters*, *376*, 29-42.

Lahr, J. C., and G. Plafker (1980), Holocene Pacific - North American plate interaction in southern Alaska: implications for the Yakataga seismic gap, *Geology*, *8*(10), 483-486.

Mackey, K. G., K. Fujita, L. V. Gunbina, V. N. Kovalev, V. S. Imaev, B. M. Koz'min, and L. P. Imaeva (1997), Seismicity of the Bering Strait region: Evidence for a Bering block, *Geology*, *25*(11), 979-982.

Page, R. A., G. Plafker, and H. Pulpan (1995), Block rotation in east-central Alaska: A framework for evaluating earthquake potential?, *Geology*(23), 4.

Plafker, G., L. M. Gilpin, and J. C. Lahr (1994), Neotectonic map of Alaska, in Plafker, George, and Berg, H.C, eds, The Geology of Alaska: Geological Society of America, 2 sheets, scale *1:2,500,000 scale*.

Ratchkovski, N. A., and R. Hansen (2002), New Constraints on Tectonics of Interior Alaska: Earthquake Locations, Source Mechanisms, and Stress Regime, *Bulletin of the Seismological Society of America*, *92*(3), 17.

Ruppert, N., K. Ridgway, J. Freymueller, R. Cross, and R. Hansen (2008), Active Tectonics of Interior Alaska: Seismicity, GPS Geodesy, and Local Geomorphology, *Active Tectonics and Seismic Potential of Alaska.*

Thatcher, W. and D. P. Hill (1991), Fault Orientations in Extensional and Conjugate Strike-Slip Environments and their Implications, *Geology,* 19: 1116-1120.

Waldhauser, F. (2012), HypoDD version 2.1b A Program to Compute Double-Difference Hypocenter Locations.

Waldhauser, F., and W. L. Ellsworth (2000), A Double-Difference Earthquake Location Algorithm: Method and Application to the Northern Hayward Fault, California, *Bulletin of the Seismolgical Society of America*, *90*(6), 1353-1368.

Yin, A. and M. H. Taylor (2008), Non-Andersonian conjugate strike-slip faults: Observations, theory, and tectonic implications, *IOP Conference Series: Earth and Environmental Science*.

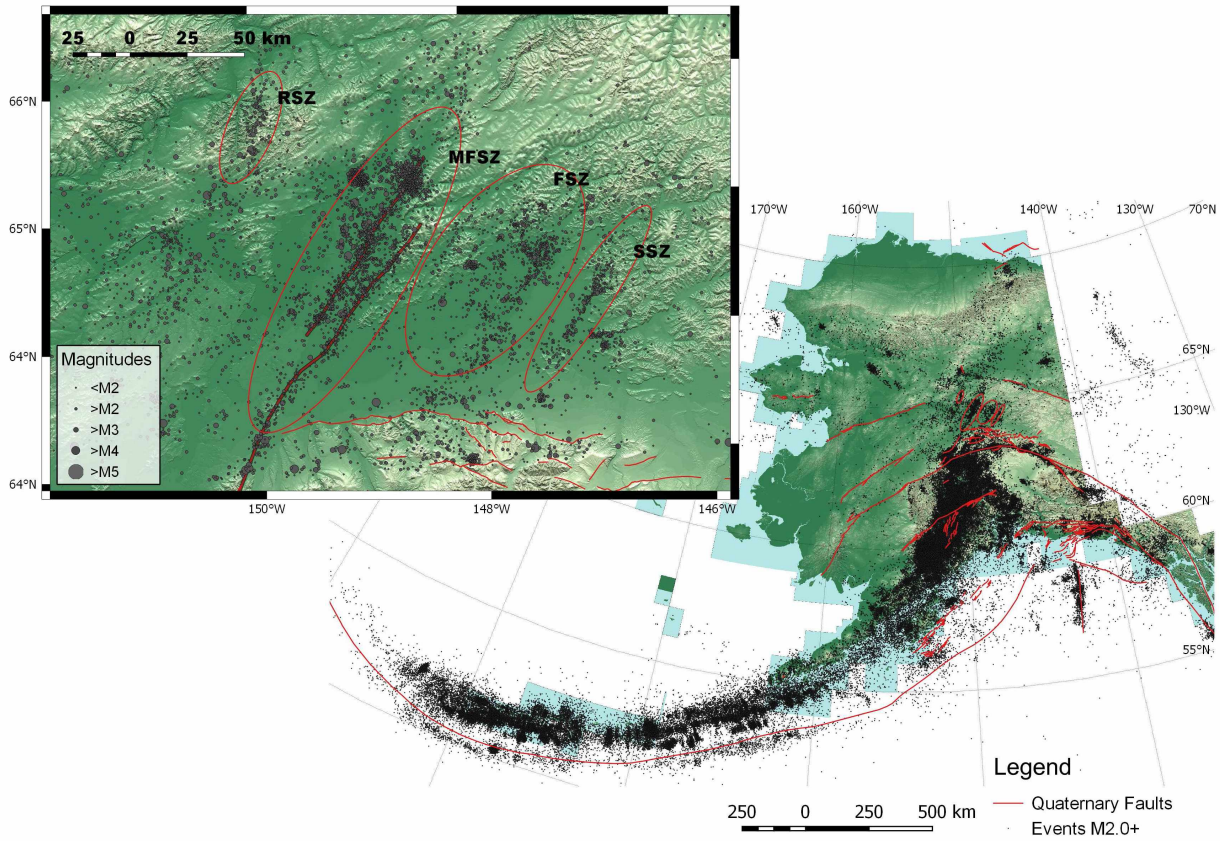

Figure 3.1 Map of Alaska and Interior Alaska Seismicity (inset).
Black dots represent earthquakes from 1975 until 2014. Red lines are mapped Holocene faults, red ovals mark seismic zones. The Interior consists of a series of seismic zones, including The Rampart Seismic Zone (RPZ), Minto Flats Seismic Zone (MFSZ), the Fairbanks Seismic Zone (FSZ), and the Salcha Seismic Zone (SSZ) from west to east. While there are no mapped faults, each seismic zone clearly consists of a series of seismic lineations that we interpret as faults.

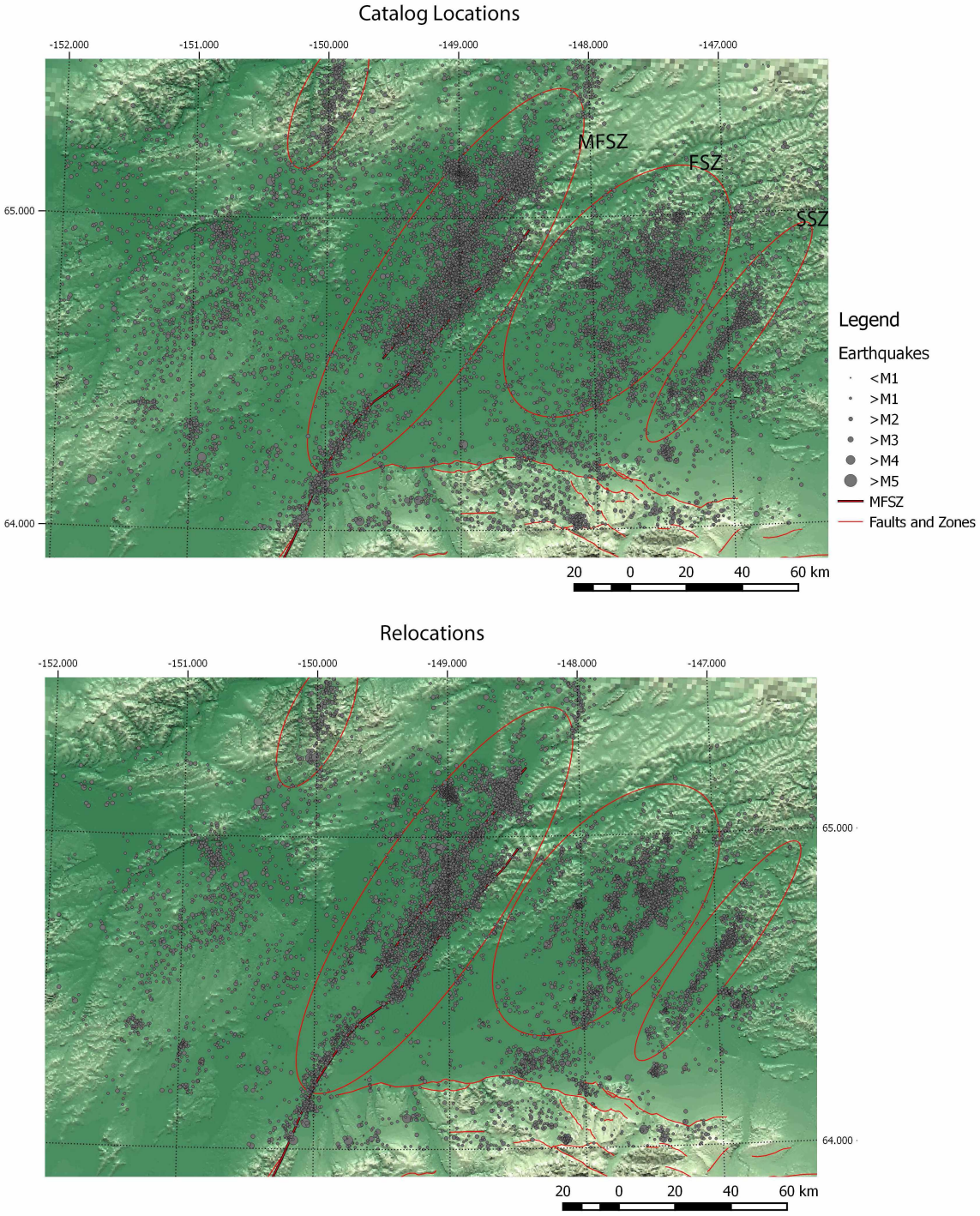

Figure 3.2 Interior Seismicity
Grey dots are earthquakes, fine red lines are mapped faults, red ovals broadly outline the seismic zones, and the thick red line is a digitized version of the MFSZ seismicity. (top) Catalog locations for all Interior earthquakes in the Alaska Earthquake Center catalog ordered from 1975-2014. (bottom) Relocated seismicity of earthquakes M 0.8 and larger.

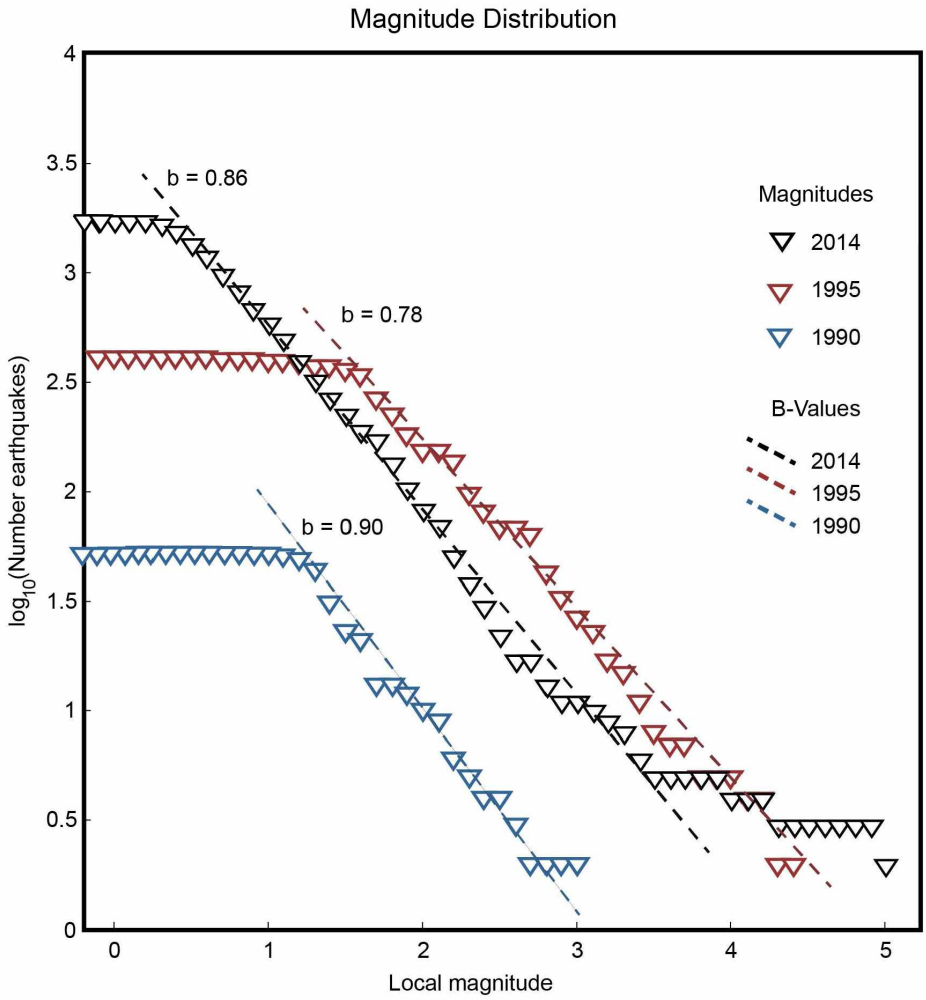

Figure 3.3 Magnitude of Completion and B-Values
Each sequence has a different magnitude of completion, based largely on the state of the network at the time. B-values are all very similar, within error of each other, and indicate that the three faults have similar properties.

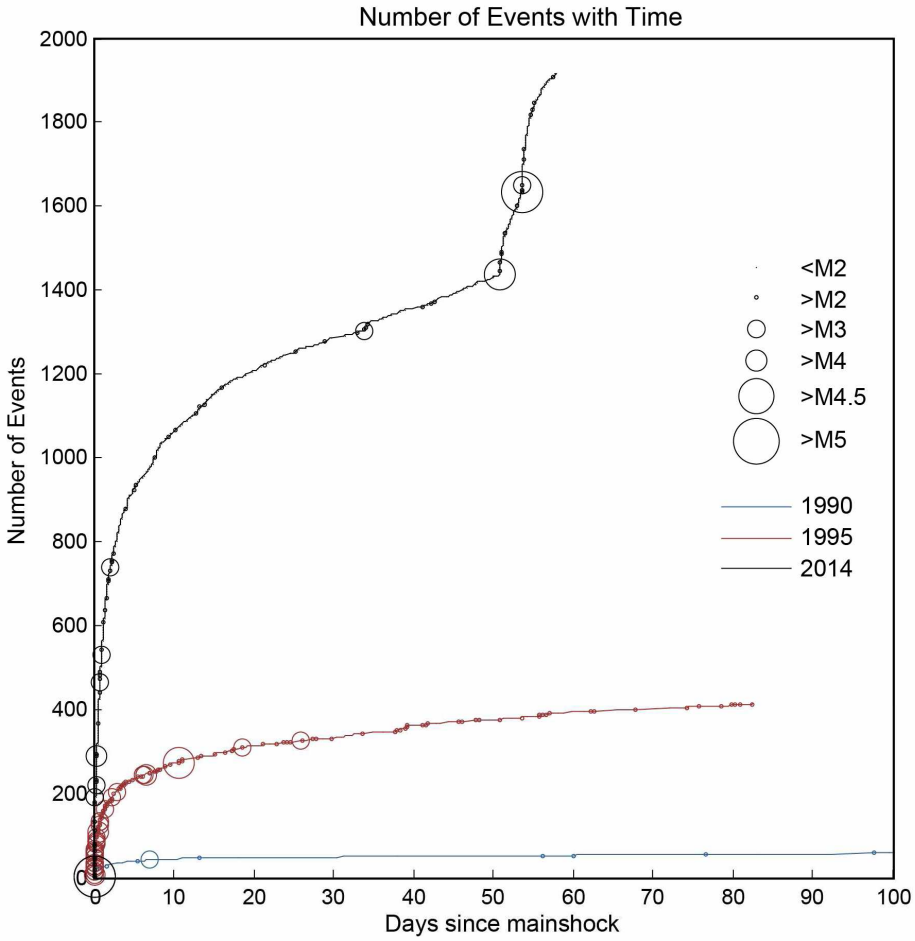

Figure 3.4 Cumulative Number of Earthquakes
The three sequences show very different numbers of recorded earthquakes. Given the magnitude of the 1995 mainshock, it is surprising that so many more earthquakes were recorded in 2014. This is probably due to a combination of improved network and the possibility that the 2014 earthquake was more productive in terms of aftershocks.

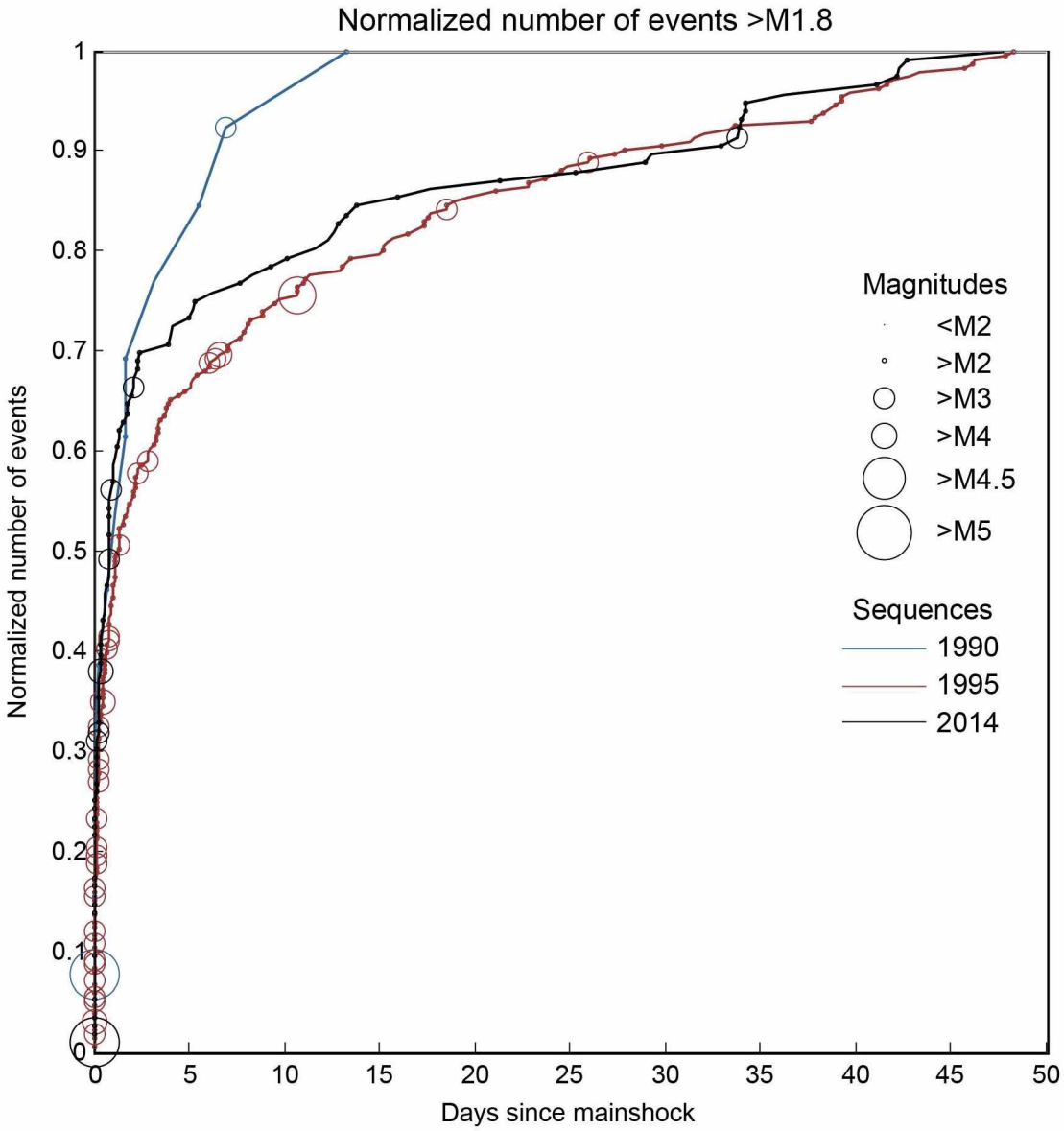

Figure 3.5 Normalized Cumulative Number of Events.
The normalized number of earthquakes greater than M1.8 (the magnitude of completeness of the 1995 sequence). The 1990 sequence has few large earthquakes and therefore quickly reaches the total number of earthquakes. The 2014 sequence includes only those earthquakes that occurred before the October M 5 earthquakes.

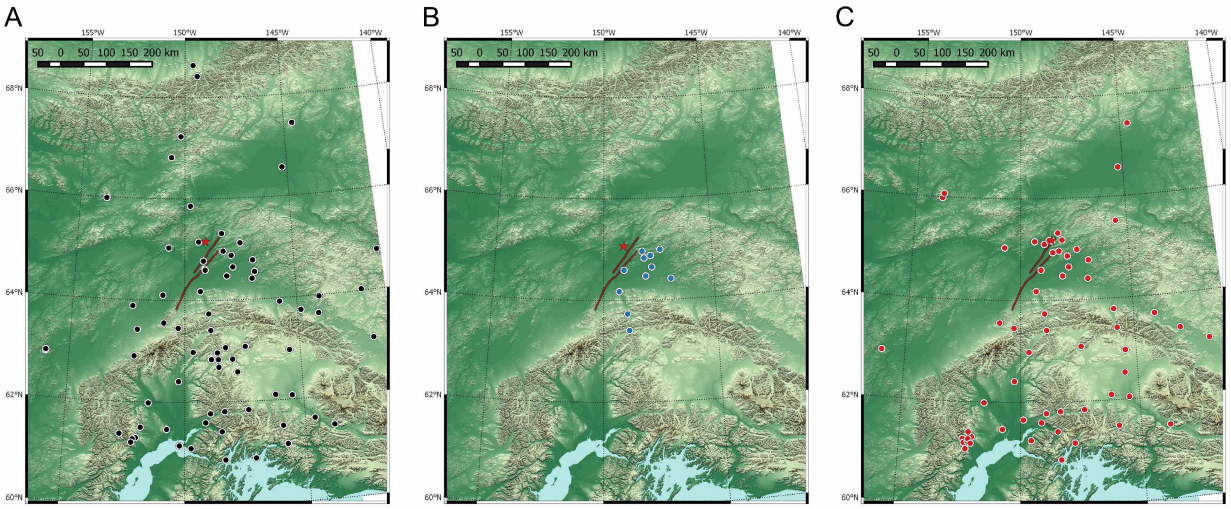

Figure 3.6 Station Coverage
(A) Stations used during relocation of the 2014 sequence. (B) Stations used for the 1990 sequence. (C) Stations used for the 1995 relocations.

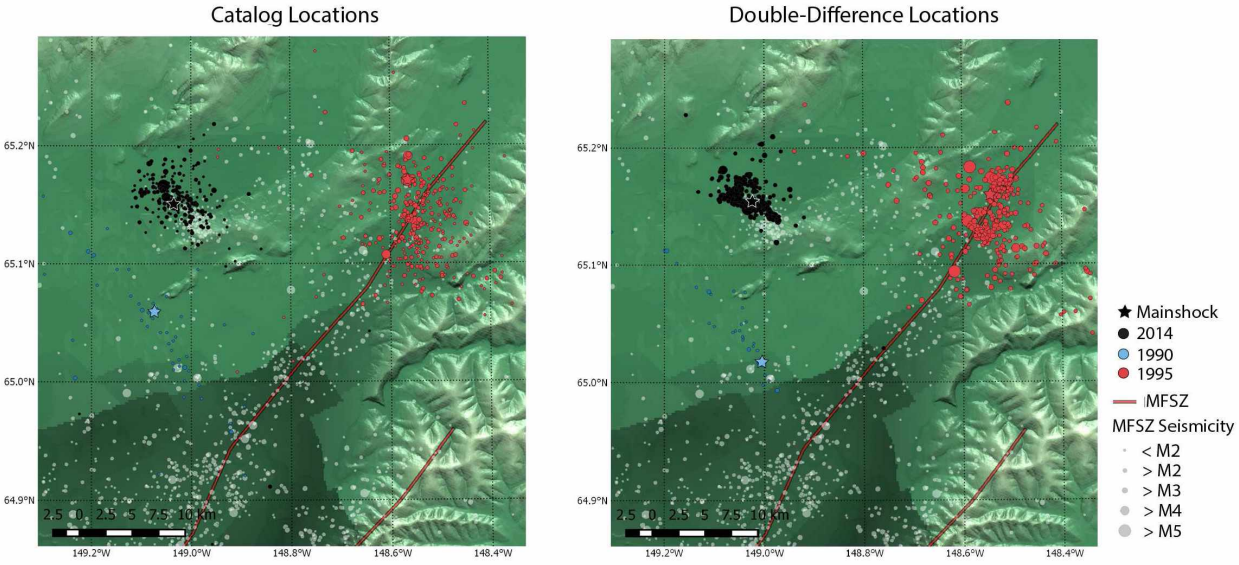

Figure 3.7 Earthquake Locations for the Minto Area Sequences.
Black: 2014; blue: 1990; red: 1995; light grey: background seismicity. Mainshocks are marked by a star. (left) Catalog locations. (right) Double-difference relocations.

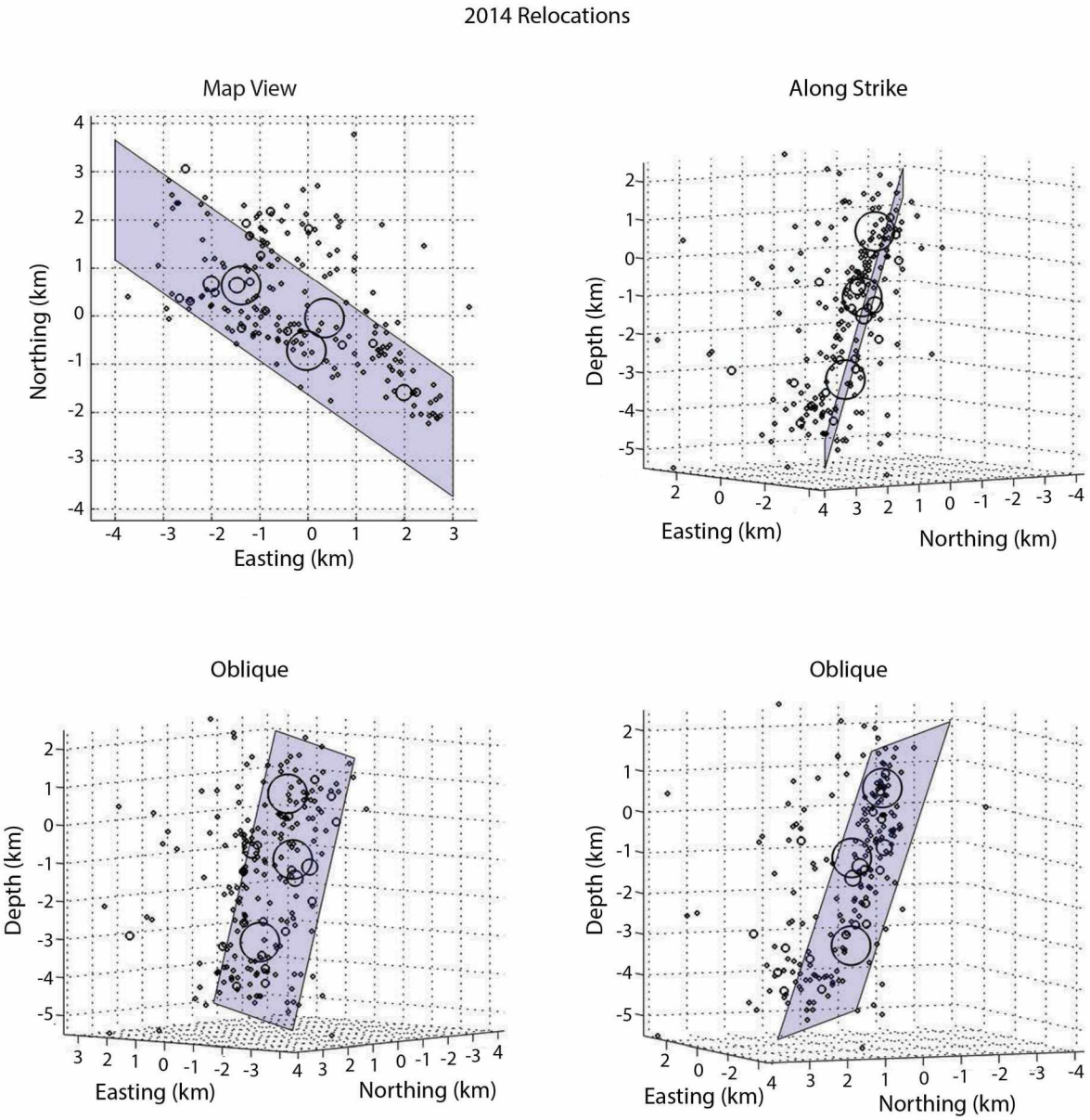

Figure 3.8 2014 Relocations
Four views of the same earthquakes and fitted plane (blue). Earthquake size indicates magnitude. Plane strikes approximately 300°, dipping 75° to the northeast.

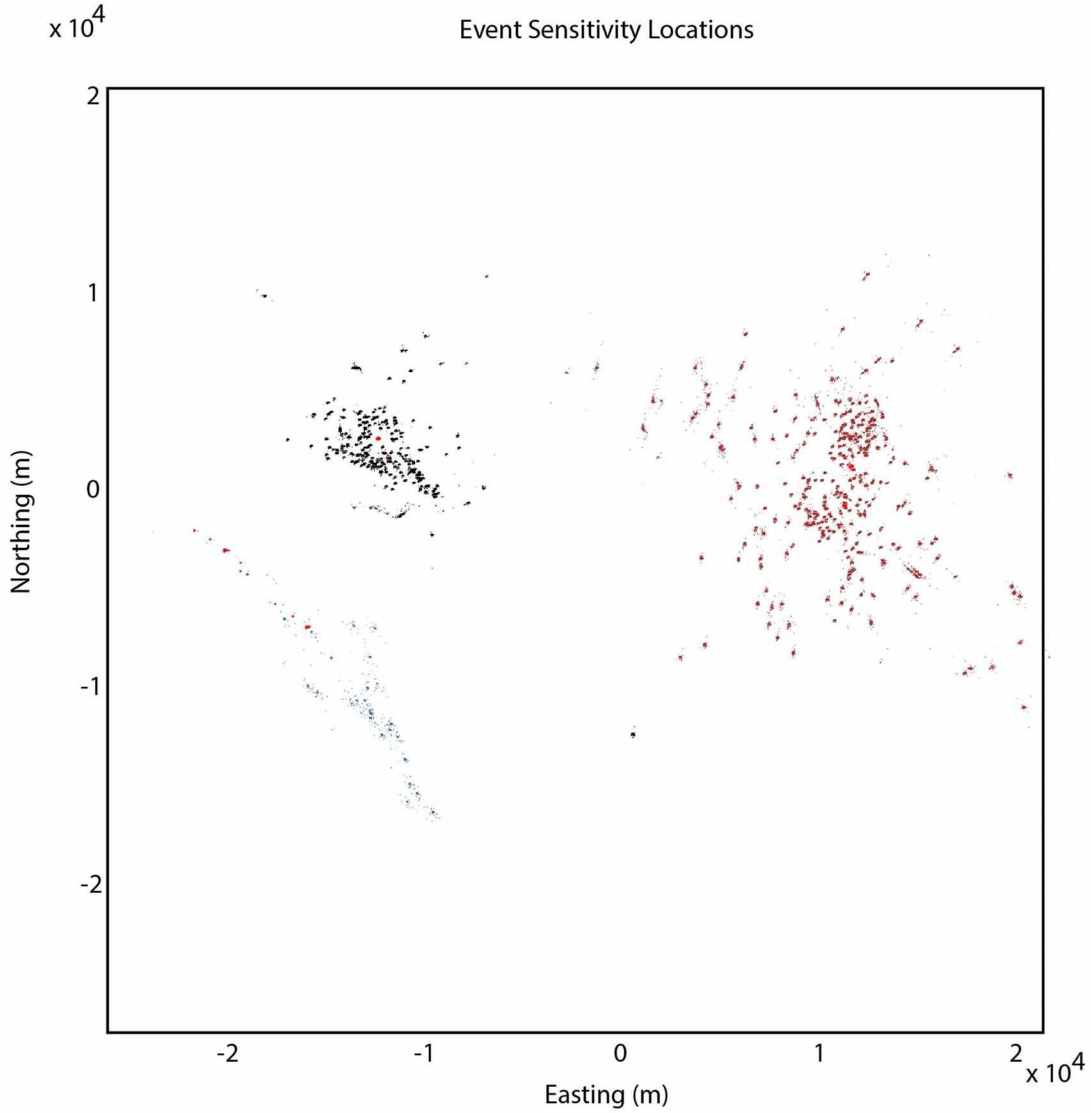

Figure 3.9 Event Sensitivity Locations.
Black: 2014 earthquake sequence; blue: 1990 earthquake sequence; red: 1995 earthquake sequence. Each earthquake is plotted 580 times, one for each event sensitivity test. This creates a small cloud of seismicity that represents a single earthquake. In bright red are randomly selected earthquakes, to highlight the "typical" spread of earthquake locations in the tests.

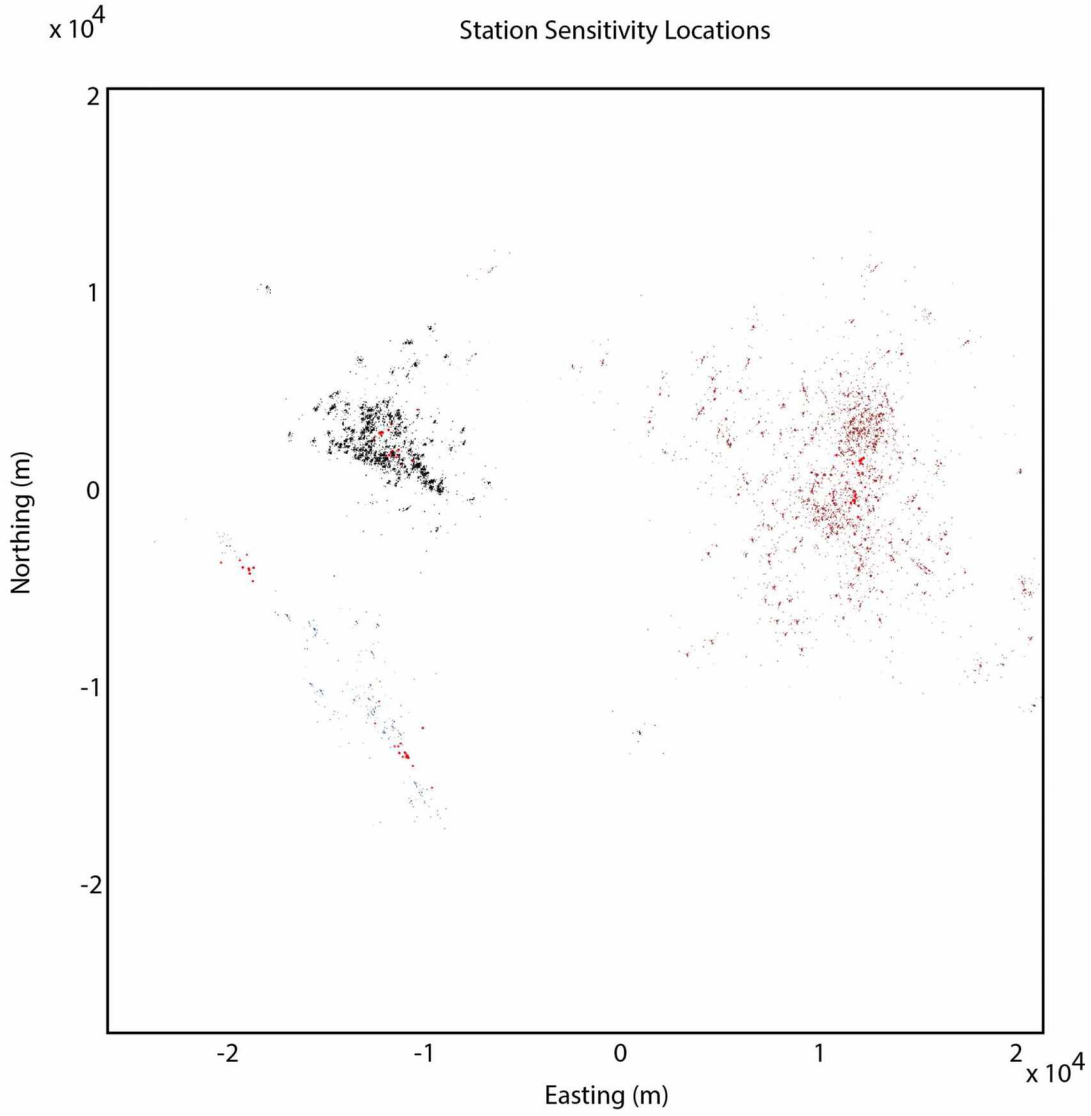

Figure 3.10 Station Sensitivity Locations.
Black: 2014 earthquake sequence; blue: 1990 earthquake sequence; red: 1995 earthquake sequence. Each earthquake is plotted 90 times, one for each station sensitivity test. This creates a small cloud of seismicity that represents a single earthquake. In bright red are randomly selected earthquakes, to highlight the "typical" spread of earthquake locations in the tests.

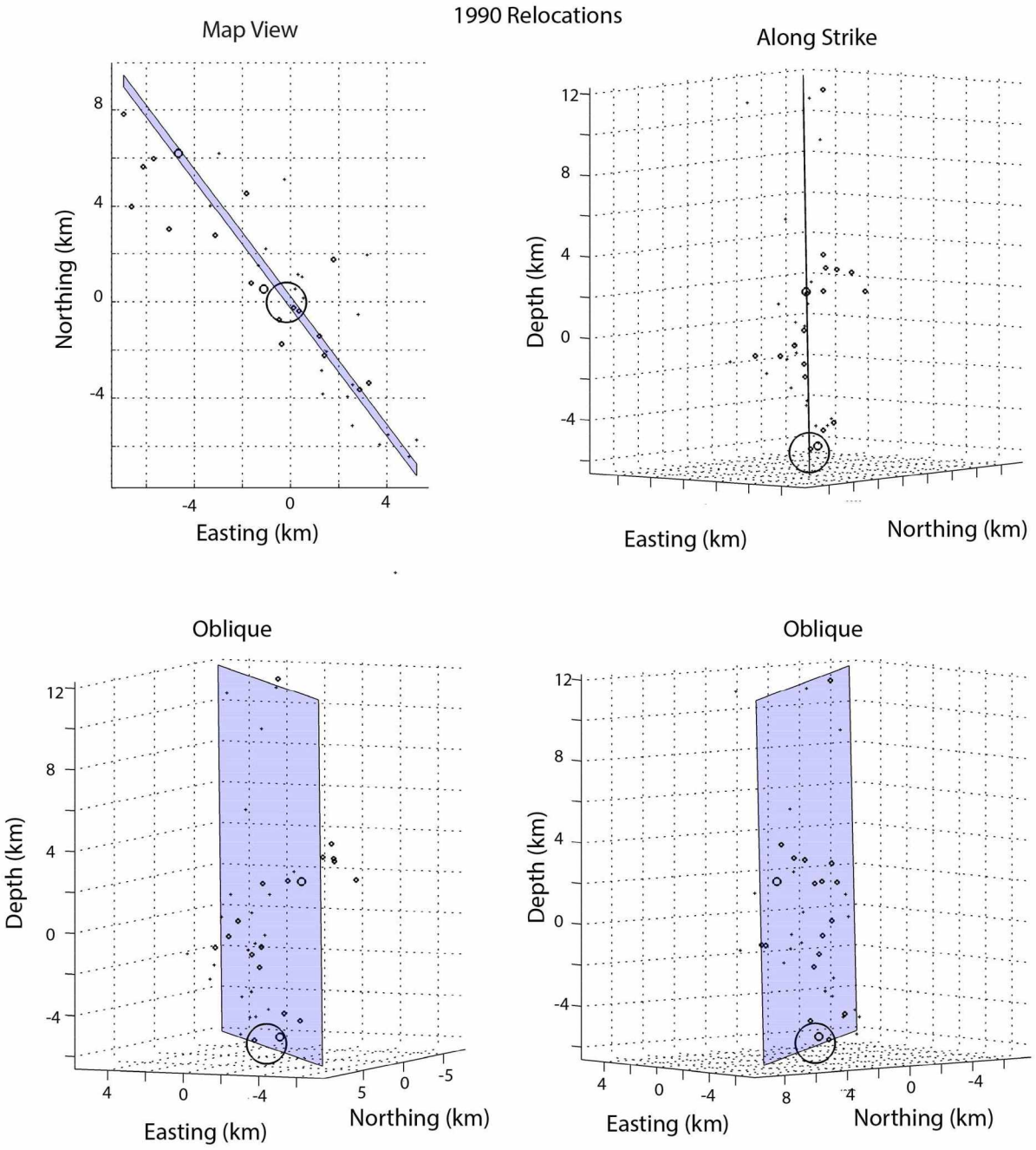

Figure 3.11 1990 Relocations
Fitted plane in blue strikes at approximately 330°, dipping nearly vertically.

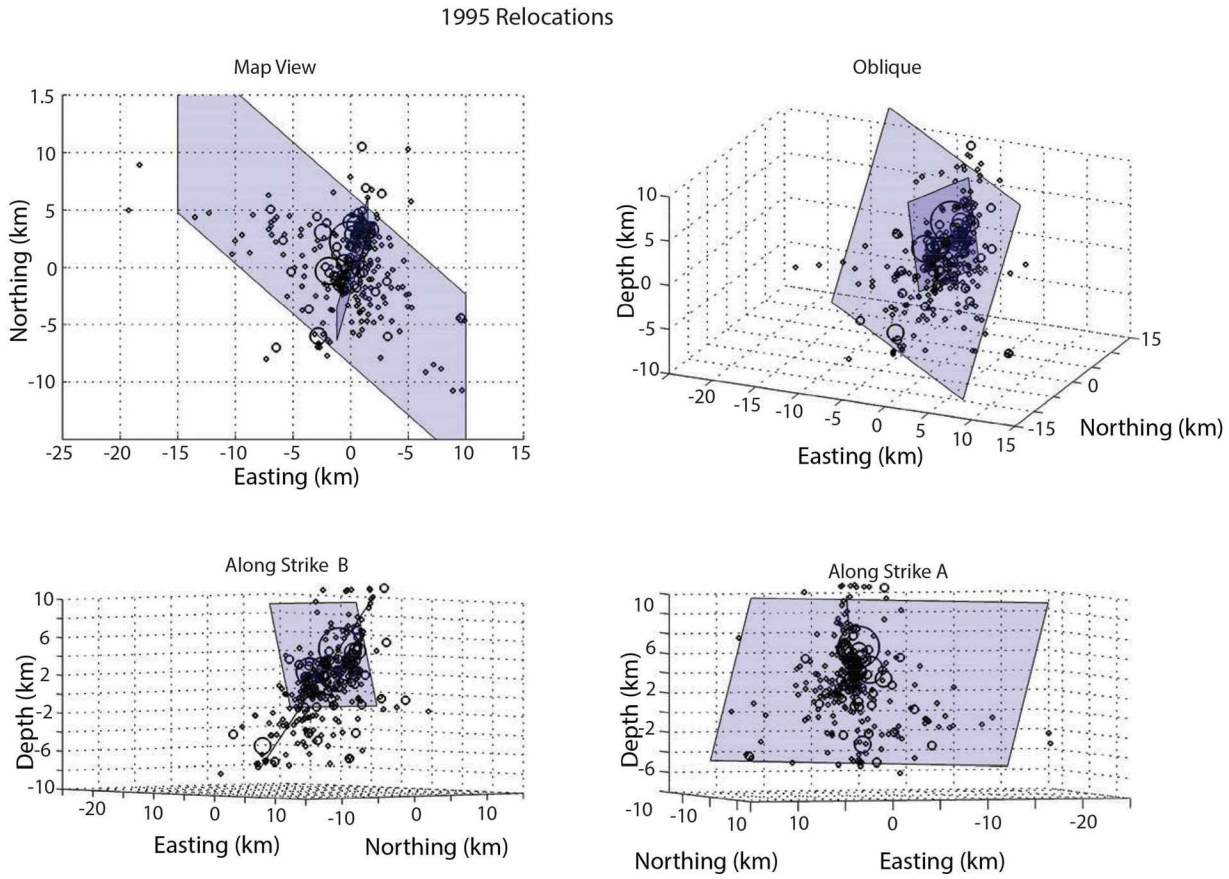

Figure 3.12 1995 Relocations
There are two planes fitted to the 1995 sequence. When all earthquakes are fit, the NW feature is highlighted in a plane that strikes approximately 320° and dips ~55° to the southwest. When just those earthquakes in the densest part of the cloud are fit, we get a nearly vertical plane that strikes approximately 10°.

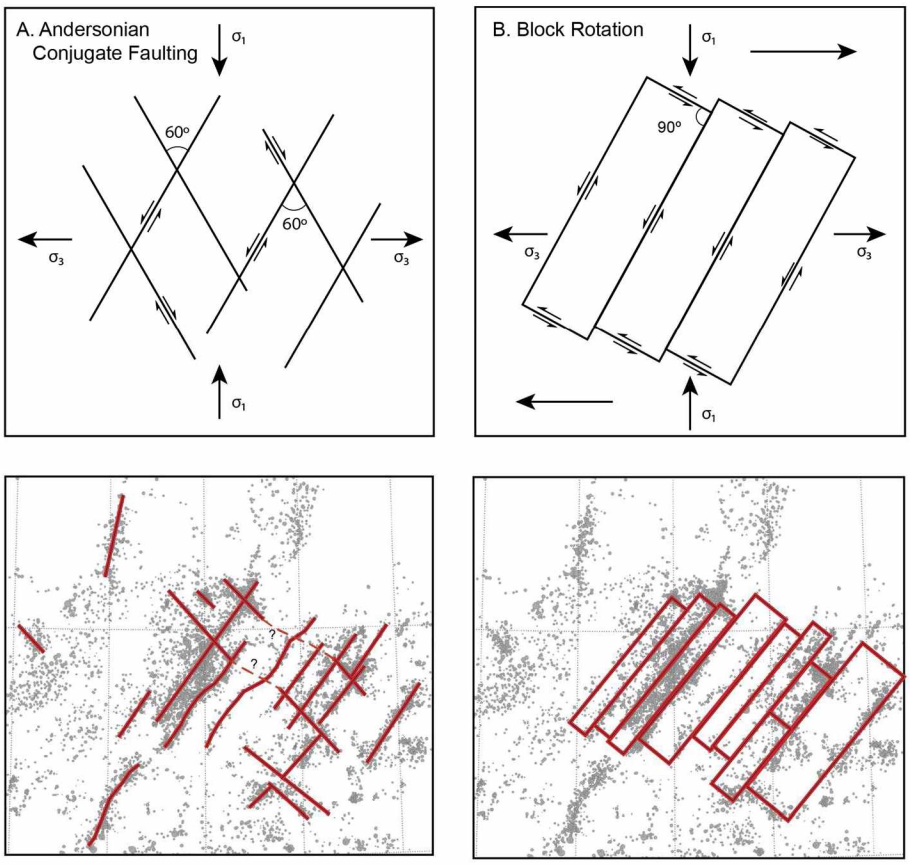

Figure 3.13 Interpretations of Seismic Patterns
(a) Conjugate faulting schematic. Faults are approximately 60° from each other and 30° from the maximum compressive stress. Sense of slip is opposite on the NW faults as the NE faults. (b) Block rotation model. All edges have left-lateral motion. (bottom) Seismic patterns with interpretations in red. The sense of slip associated with the block model is opposite the observed sense of slip on the NW-striking faults, indicating that it cannot be the source of the cross-faults.

Table 3.1Velocity Model
We used a modified version of the N. Alaska velocity model used by the Alaska Earthquake Center, with a Vp/Vs of 1.76

Layer depth (km)	P-velocity
0	4.9
24	7.4
40	7.9
76	8.29
301	10.4
545	12.6

Table 3.2 Sensitivity Test Results.
Standard deviations of the positional shifts in the X (north), Y (east), and Z (vertical) directions.

		X (m)	Y (m)	Z (m)
2014	Event	56	39.6	223
	Station	133.4	128.6	390.4
1990	Event	78	91	225.3
	Station	258.2	250.7	781
1995	Event	98.9	152.2	302.8
	Station	314.2	465.4	587.2

Conclusion

This thesis used seismic patterns in two very different environments – Uturuncu volcano and Interior Alaska – to improve our understanding of the mechanism of deformation. By using the double-difference method and incorporating cross-correlations, I was able to produce high-resolution relative earthquake locations, which I in turn used to analyze the processes generating the earthquakes.

At Uturuncu, I found that there is a layer of convex-upward seismicity at 5-10 km beneath the surface with little to no seismicity below it. Given gravity (del Potro *et al.*, 2013) and seismic data (West *et al.*, 2013) that suggest lobes of low-density, low-velocity material, and the good alignment between the band of seismicity and the low velocity zone found in seismic tomography studies, I suggest that the seismicity recorded beneath Uturuncu volcano is related to the top of a diapir. Additionally, I find that the orientations of fault planes for families of repeating earthquakes around the volcano fall into a radial pattern. Such a pattern suggests that the stresses producing the seismicity are related to inflation at the volcano rather than regional stresses. This couples well with studies that have shown that many of the earthquakes recorded have a significant component of non-double couple motion (Alvizuri and Tape, 2014). Such motion is likely due to fluid movement at depth, likely sourced from the magma below.

In Alaska's Interior, I relocated nearly 40 years worth of seismicity and found that in addition to the previously recognized NE-striking faults, there is a series of NW-striking faults. The 60° angles between the faults suggest that they are conjugate faults, as does the sense of motion. I also examined three earthquake sequences that occurred near the northern end of the Minto Flats Seismic Zone. Two of the three sequences took place on WNW-striking faults, while one ruptured along a NNE-striking fault. The latter earthquake did produce aftershocks in a NW-SE halo, suggesting that the rupture may have produced stress changes that cause the nearby, broken and blocky crust to readjust. The focal mechanisms of the two NW-striking earthquakes indicate dextral motion. Such motion is counter to that expected in the block rotation model and also suggests that they are a part of a conjugate fault system.

Though in two very different environments, I have managed to improve our understanding of the processes at play through the use of earthquake relocations.

References

Alvizuri, C. and C. Tape (2014), Full Moment Tensors for Small (Mw<3) Events at Uturuncu Volcano, Bolivia, *Seismological Society of America Annual Meeting*, Anchorage, AK.

del Potro, R., M. Diez, J Blundy, and A.G. Camacho. (2013), Diapiric ascent of silicic magma beneath the Bolivian Altiplano, *Geophysical Research Letters*, 40(10): 2044-2048.

de Silva, S. L. (1989, Altiplano-Puna volcanic complex of the central Andes, *Geology*, 17: 1102-1106.

Page, R. A., G. Plafker, and H. Pulpan (1995), Block rotation in east-central Alaska: A framework for evaluating earthquake potential?, *Geology*, (23): 4

Pritchard, M. E. and M. Simons (2002), A satellite geodetic survey of large-scale deformation of volcanic centers in the central Andes, *Nature*, 418(6894): 167-171.

Sparks, R. S. J., C. B. Folkes, M. C. S. Humphreys, D. N. Barford, J. Clavero, M. C. Sunagua, S. R. McNutt, and M. E. Pritchard (2008), Uturuncu volcano, Bolivia: Volcanic unrest due to mid-crustal magma intrusion, *American Journal of Science*, 308(6): 727-769.

West, M. E., E. Kukarina, and I. Koulakov (2013), Structure of Uturuncu Volcano from Seismic Tomography, *American Geophysical Union Fall Meeting 2013*, San Francisco, CA.

Appendix

Permission for the use of manuscripts in this thesis.

Carl Tape <ctape@alaska.edu> Fri, Aug 7, 2015 at 11:23 AM

To: Laura Hutchinson <lkhutchinson@alaska.edu>

Hi Laura,

I, Carl Tape, give Laura Hutchinson permission to include the manuscript "Double-Difference Relocation of Interior Alaska Earthquakes" in her thesis entitled "Double-Difference Relocation of Earthquakes at Uturuncu Volcano, Bolivia, and Interior Alaska".

Carl

Carl Tape
Assistant Professor
Geophysical Institute (office 413D)
University of Alaska Fairbanks
Phone: 907-474-5456
Email: ctape@alaska.edu
Web: http://www.giseis.alaska.edu/input/carl/

Celso Alvizuri <alvizuri@gi.alaska.edu> Thu, Aug 6, 2015 at 4:10 PM

To: Laura Hutchinson <lkhutchinson@alaska.edu>

Hi Laura,

I, Celso Alvizuri, give Laura Hutchinson permission to include the manuscript "Double-Difference Relocation of Earthquakes at Uturuncu Volcano, Bolivia " in her thesis entitled "Double-Difference Relocation of Earthquakes at Uturuncu Volcano, Bolivia, and Interior Alaska".

Celso